Gasoline surrogate oxidation in a motored engine, a JSR, and an RCM: Characterization of cool-flame products by high-resolution mass spectrometry

Nesrine Belhadj, Maxence Lailliau, Zahraa Dbouk, Roland Benoit, Bruno Moreau, Fabrice Foucher, Philippe Dagaut

Gasoline surrogate oxidation in a motored engine, a JSR, and an RCM: Characterization of cool-flame products by high-resolution mass spectrometry

Nesrine Belhadj[a,b], Maxence Lailliau[a,b], Zahraa Dbouk[a], Roland Benoit[a], Bruno Moreau[b], Fabrice Foucher[b], Philippe Dagaut[a,*]

[a]*Centre National de la Recherche Scientifique, INSIS, Institut de Combustion, Aérothermique, Réactivité, Environnement, 45071 Orléans, France*
[b]*Université d'Orléans, Laboratoire PRISME, 8 Rue Léonard de Vinci, 45100 Orléans, France*

*Corresponding author:

Philippe Dagaut

CNRS–ICARE, Institut de Combustion, Aérothermique, Réactivité et Environnement

1C Avenue de la Recherche Scientifique - 45071 Orléans Cedex 2, France

Tel: +33 (0)2 38 25 54 66 - dagaut@cnrs-orleans.fr

ABSTRACT: The oxidation of a PRF 50 gasoline surrogate (*n*-heptane/iso-octane) performed earlier in a jet-stirred reactor (JSR) and a rapid compression machine (RCM), showed that oxidation proceeds similarly in both conditions. The present work extends that investigation by oxidizing a *n*-heptane / iso-octane mixture under motored engine conditions. Exhaust gases were collected through bubbling in cooled acetonitrile. The samples were analyzed by ultra-high-pressure liquid chromatography (UHPLC) coupled to high-resolution mass spectrometry (HRMS-orbitrap Q-Exactive™). Low-temperature oxidation intermediates were characterized using tandem mass spectrometry (MS/MS), H/D exchange, and 2,4-dinitrophenyl hydrazine derivatization. In addition to cyclic ethers/ketones/aldehydes ($C_7H_{14}O$, $C_8H_{16}O$), ketohydroperoxides ($C_7H_{14}O_3$, $C_8H_{16}O_3$), diketones ($C_7H_{12}O_2$, $C_8H_{14}O_2$), and keto-dihydroperoxides ($C_7H_{14}O_5$, $C_8H_{16}O_5$), presented in our previous work, a large set of newly detected or rarely considered low-temperature products are presented here. They include hydroperoxides and diols ($C_7H_{16}O_2$, $C_8H_{18}O_2$), olefinic hydroperoxides/diols ($C_7H_{14}O_2$, $C_8H_{16}O_2$), dihydroperoxides ($C_7H_{16}O_4$, $C_8H_{18}O_4$), olefinic dihydroperoxides ($C_7H_{14}O_4$, $C_8H_{16}O_4$), olefinic cyclic ethers/carbonyls ($C_7H_{12}O$, $C_8H_{14}O$), di- and tri-olefinic cyclic ethers/ketones/aldehydes ($C_7H_{10}O$, C_7H_8O), olefinic ketohydroperoxides ($C_7H_{12}O_3$, $C_8H_{14}O_3$), di-olefinic ketohydroperoxides ($C_7H_{10}O_3$), triketones ($C_7H_{10}O_3$, $C_8H_{12}O_3$), olefinic diketones ($C_7H_{10}O_2$, $C_8H_{12}O_2$), di-olefinic diketones ($C_7H_8O_2$), and diketo-hydroperoxides ($C_7H_{12}O_4$, $C_8H_{14}O_4$). Motored engine's low-temperature oxidation intermediates were compared to those obtained in JSR and RCM. Despite the strong differences in the experimental conditions, the results indicate the formation of the same products. This indicates that a common chemical mechanism operates in motored engine, JSR, and RCM.

Keywords: low-temperature oxidation; motored engine, jet-stirred reactor; rapid compression machine; liquid chromatography; high-resolution mass spectrometry

1. INTRODUCTION

The primary reference fuels (PRFs), *n*-heptane and iso-octane, with a research octane number (RON) of 0 and 100, respectively, are the most widely used gasoline surrogate components. *n*-Heptane/iso-octane mixtures with RON>30 can show strong low-temperature chemistry[1]. Studying the formation of PRFs low-temperature oxidation intermediates has been the topic of research for several decades. Dagaut et al.[1] studied the oxidation of *n*-heptane/iso-octane blends in a jet-stirred reactor, JSR, (RON=10 to 90, 550-1150 K, 10 atm, φ=1). Their results showed the formation of a large variety of species, including C_7 and C_8 cyclic ethers (2-methyl-5-ethyl-tetrahydrofuran, 2,2,4,4-tetramethyl-THF, 2-propyl-THF, and 3,3-dimethyl-oxetane). More recently, Chen et al. [2] investigated the oxidation of PRF 70 under JSR conditions (520-710 K, 700 torr, φ=0.5). They used time-of-flight molecular beam mass spectrometry with photoionization by synchrotron vacuum-ultraviolet light (SVUV-TOF-MBMS) to identify low-temperature intermediates, e.g., keto-hydroperoxides (KHPs), olefinic and di-olefinic KHPs, and other saturated and unsaturated oxygenated species ($C_7H_{10,12,14}O_{1,2}$, $C_8H_{14,16}O$, $C_8H_{14}O_2$). The formation of low-temperature oxidation species of PRFs mixture was also studied using a Cooperative Fuel Research (CFR) motored engine. Filipe et al.[3] used a non-dispersive infrared (NDIR) analyzer to measure exhaust carbon monoxide (CO) formed in a motored engine. The other stable intermediates (carbon dioxide, C_4-alkenes, formaldehyde, methanol etc.) were measured by gas chromatography coupled to a flame ionization detector (GC-FID). Leppard et al.[4] investigated the auto-ignition chemistry of PFRs binary blends in a motored engine (speed of 900 rpm, intake manifold of 60 kPa, and intake temperature of 359 K). Exhausts were condensed in a trap immersed in a dry ice-isopropanol bath. Samples were analyzed by GC-MS and GC-FTIR (Fourier-transform infrared spectroscopy), which allowed them to identify stable species (C_7 and C_8 oxygenated heterocycles, carbonyls, conjugated alkenes etc.). The authors used the 2,4-dinitrophenyl hydrazine (DNPH) derivatization to quantify formaldehyde. Concerning the oxidation of PRFs in rapid compression machines (RCM), oxidation intermediates deriving from *n*-heptane and iso-octane have been studied previously[5-8]. However, besides in our previous study[9], no probing of fuel-specific oxidation intermediates of *n*-heptane/iso-octane mixtures has been performed earlier in RCM. In that study[9], we observed the formation of a wide range of low-temperature oxidation products, e.g., hydroperoxides, diols, ketohydroperoxides (KHPs), carboxylic acids, diketones, cyclic ethers ($C_nH_{2n}O$), and highly oxidized compounds produced through up to six O_2 additions on alkyl radicals ($C_nH_{2n}O_{11}$). However, compounds such as olefinic hydroperoxides, olefinic dihydroperoxides, olefinic cyclic ethers/ketones/aldehydes, di- and tri-olefinic cyclic ethers/carbonyls, olefinic KHPs, di-olefinic KHPs, triketones, olefinic and di-olefinic diketones have not been reported.

The present experimental investigation extends from that previous work[9]. Here, we focus on comparing low-temperature species formed in a motored engine, with experimental data obtained in JSR and RCM experiments. We also probe low-temperature intermediates not reported before. Experiments

were carried out in a modified homogeneous compression ignition (HCCI) motored engine type DW10. Exhausts gases were bubbled in cooled acetonitrile (ACN). The samples were analyzed by ultra-high-pressure liquid chromatography (UHPLC) coupled to atmospheric pressure chemical ionization (APCI) and high-resolution mass spectrometry (HRMS). Specific chemical functions (hydroperoxy and carbonyl) of low-temperature oxidation intermediates, were characterized by H/D exchange and DNPH derivatization methods, already used in previous studies focusing on the characterization of fuel's oxidation products [10-15] .

2. EXPERIMENTS

The oxidation of a PRF 50 mixture, i.e., 50 % *n*-heptane and 50% iso-octane in volume (fuels purity: >99.5 %, from Sigma-Aldrich®), was carried out under cool flame conditions. Three experimental systems were used: a motored engine, a JSR, and an RCM.

2.1. HCCI motored engine. The engine used in this study is a single-cylinder conventional Diesel engine (DW10 from PSA®), modified to run in HCCI mode. The engine parameters are given in Table 1. An electric motor was used to maintain a constant rotation speed, as presented in a schematic of the experimental apparatus (Figure 1). Mass flow controllers (Emerson® for air, Brooks® for nitrogen, and Bronkhorst® for PRF 50) were used to control flows of gases and liquid fuel, and to introduce a homogeneous PRF50/air mixture inside a plenum upstream of the combustion chamber. N_2 coming from a nitrogen generator, and air coming from air compressor, were dried at -40 °C dew point to avoid ice formation during the sampling. In order to maintain the cool flame close to the top dead center, and to quench the main flame during the expansion stroke, intake pressure and temperature collector were regulated at 1.5 bar and 23 °C, respectively. Then, the high-temperature ignition is avoided, allowing to probe the formation of low-temperature oxidation products under engine conditions. An electric resistor was used to maintain a constant temperature close to the intake valves. As shown in Figure 1, exhausts gases were sampled by bubbling in 15 ml of cooled acetonitrile (ACN from Carlo Erba®) during 20 min. (sampled volume: 100 L). To this end, a midget bubbler (from Supelco®) and a paraffin oil bath maintained at -35 °C, were used. Back pressure was regulated at 1.05 bar to allow exhausts gas flow through the bubbler. As in previous works [9, 16-18], liquid samples were stored in a freezer at -15 °C for HRMS analyses.

Table 1. Motored engine specification and operating conditions

Engine parameter (units)	Value
Bore (mm)	85
Stroke (mm)	88
Connecting rod (mm)	145
Geometric compression ratio (-)	9.2
Speed (rpm)	1500
Intake manifold pressure (kPa)	95
Global equivalence ratio (-)	0.5

Oxygen concentration (%)	20

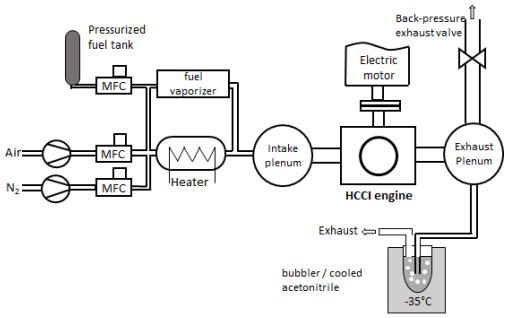

Figure 1. The HCCI motored engine experimental setup showing the trapping system at the exit of the exhaust plenum.

Typical recordings of in-cylinder pressure, temperature, and heat release rate as a function of crank angle (CAD) are presented in Figure 2. One can see that the pressure in the cylinder reached a maximum of ~22 bar and the temperature increased to ~690 K. A low-temperature heat release of ~8 J/CAD, was measured.

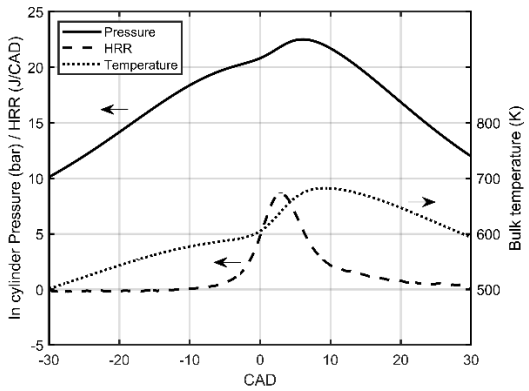

Figure 2. In-cylinder pressure, temperature, and heat release rate (HRR) recorded as a function of crank angle degree (CAD), during low-temperature oxidation of PRF 50 under HCCI motored engine conditions

2.2. Jet-stirred reactor (JSR). A description of the jet-stirred reactor set-up has been published elsewhere [9, 19-21]. It has been successfully used to study the oxidation of a range of hydrocarbon mixture and commercial fuels[1, 22]. In short, it consists of a fused silica sphere (volume 42 cm^3) containing 4 injectors (nozzles of 1 mm I.D). The 4 jets from the injectors provide stirring. An HPLC pump (LC10 AD VP from Shimadzu®) was used to send the fuel to the JSR, and mass flow meters (Brooks™) were used to regulate flow rates of N_2 and O_2. The PRF 50/N_2 and O_2/N_2 mixtures were injected separately to avoid oxidation before reaching the injectors. A Pt-Pt/Rh-10% thermocouple was used to measure the temperature inside the JSR. Gas samples from a fused silica probe were bubbled for 75 min in 25 mL cooled ACN (sampled volume: 45 L). As before[9], the resulting liquid samples were stored in a freezer

at -15 °C for further chemical analyses. Experimental conditions for the oxidation of a PRF 50 mixture in JSR and RCM, are summarized in Table 2.

Table 2. Experimental conditions for the oxidation of a PRF 50 mixture in JSR and RCM

JSR	RCM
Reactive mixture: 0.5% PRF50, 12.5% O_2, 87% N_2	Reactive mixture: PRF50/air (21% O_2, 79% N_2)
Equivalence ratio (φ): 0.5	Equivalence ratio (φ): 0.5
Residence time: 1.5 s	Compression time: <4 ms
Pressure: 10 atm	Pressure: 20 bar*
Temperature 560-700 K	Temperature: 620 K

*For RCM experiments, a higher pressure was used to obtain enough fuel conversion

2.3. Rapid compression machine (RCM). The RCM setup and sampling procedure have been presented previously[9]. It allows fast compression of fuel/air mixture. Increasing pressure and temperature initiates chemical reactions causing ignition. Mass flows were controlled by Bronkhorst® Cori-Flow™ M13. A Keller® PA-33X/80794 highly precise pressure transmitter was used to measure intake pressure, and an AVL QH32C® piezoelectric pressure transducer was used to measure in-cylinder pressure. Temperatures were measured by K-type thermocouples. An orifice located at the endwall of the RCM was opened for sampling gases into a pre-evacuated stainless-steel cylinder (Swagelok®). 40 mL of ACN were used to dissolve gases contained in the sampling cylinder (sampled volume: 0.5 L). Resulting liquid samples were stored in a freezer at -15 °C.

2.4. Chemical analyzes. Identification of cool flame intermediates formed during the low-temperature oxidation of a PRF 50 mixture, under JSR, RCM, and motored engine conditions, was carried out by combining UHPLC with APCI/HRMS (Orbitrap Q-Exactive™). This HRMS can reach a resolution of 140,000 at *m/z* 200, and a high mass accuracy (< 1 ppm). Thereby we were able to distinguish between species having very close exact mass, e.g., $C_9H_7O_2^+$ (*m/z* 147.04349), $C_6H_{11}O_4^+$ (*m/z* 147.06467), $C_{10}H_{11}O^+$ (*m/z* 147.07990), $C_7H_{15}O_3^+$ (*m/z* 147.10141), and $C_8H_{19}O_2^+$ (*m/z* 147.13742). Chromatographic conditions were as follows: a reversed phase column (RP-C_{18} Luna Omega from Phenomenex®, 100 mm, 2.1 mm, 1.6 µm), a mobile phase containing water (from Fisher chemical Optima®) + ACN, a gradient of 0 to 85% of ACN, and a flow rate of 250 µl/min during 20 min. In order to achieve an exhaustive identification, positive ($[M+H]^+$) and negative ($[M-H]^-$) APCI modes, were used. Low-temperature oxidation intermediates were identified using tandem mass spectrometry (MS/MS) with a higher-energy collision-induced dissociation (HCD) of 10 eV. In addition, hydroperoxy functions (OOH) were characterized by H/D exchange. To this end, 300 µL of deuterated water (D_2O 99.8 %, from Sigma-Aldrich®) were added to 1 mL of sample. The reaction time was 20 min at room temperature. Carbonyl functions (C=O) were characterized by DNPH (from Sigma-Aldrich®)

derivatization. 50 µL of a saturated solution (2 g of 2,4-DNPH in 100 mL of ACN) and 20 µL of phosphoric acid (from Sigma-Aldrich®) were added to 1 mL of oxidation samples. The reaction time was 4 hours at room temperature.

3. RESULTS

3.1. Hydroperoxides or diols ($C_7H_{16}O_2$, and $C_8H_{18}O_2$) and di-hydroperoxides ($C_7H_{16}O_4$). Several studies have highlighted the formation of peroxidic compounds during *n*-heptane oxidation in flow systems[23], motored engines[24-27], and JSRs[28]. Hydroperoxides can be formed during alkane's low-temperature oxidation via well-established combustion chemistry reactions: fuel (RH) + $X^\bullet$ ($^\bullet OH$, $HO_2^\bullet$, $H^\bullet$, $O^\bullet$ …) → $R^\bullet$ + XH; $R^\bullet + O_2 \rightarrow ROO^\bullet$; $ROO^\bullet + HO_2 \rightarrow ROOH + O_2$. Thanks to the use of a UHPLC C_{18} column coupled to negative mode APCI and HRMS, signals corresponding to $C_7H_{16}O_2$ and $C_8H_{18}O_2$ were detected in JSR, RCM, and motored engine experiments ($C_7H_{15}O_2^-$ with *m/z* 131.1076, and $C_8H_{17}O_2^-$ with *m/z* 145.1232), as shown in Figure 3a,b. It can be seen that the UHPLC analyses indicated the presence of several $C_7H_{15}O_2^-$ and $C_8H_{17}O_2^-$ chromatographic peaks, which might correspond to hydroperoxides and diols intermediates. One can note that the signal intensity obtained for the JSR sample is higher than those of motored engine and RCM. This can be explained by the decomposition of these intermediates on metallic surfaces of the motored engine and RCM. The presence of both hydroperoxides and diols species was confirmed by H/D exchange tests. An example is presented in Figure 3c. For $C_8H_{18}O_2$ species, two H/D exchanges were observed. Diols were identified at retention times of 14.12, 14.52, 14.65, 15.25, 15.32, 15.62, and 16.70 min. H/D exchange on hydroperoxides could only yield a single-deuterated ion, as observed at retention times of 15.45, 15.56, 15.83, and 16.59 min.

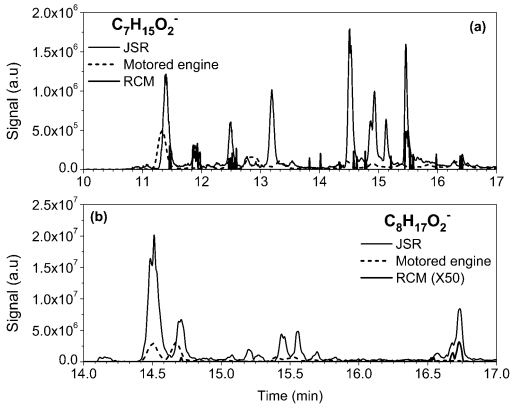

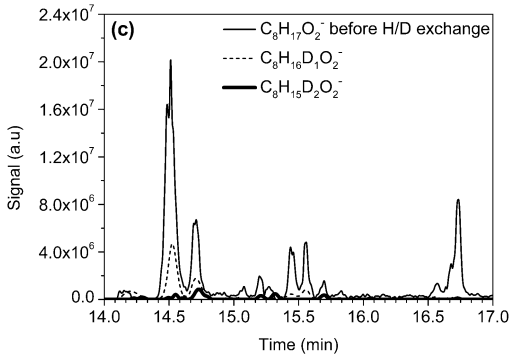

Figure 3. UHPLC-negative APCI-HRMS signal of (a) $C_7H_{15}O_2^-$ and (b) $C_8H_{17}O_2^-$ formed during low-temperature oxidation of PRF 50 in JSR (600 K), motored engine, and RCM. (c) comparison between signal of $C_8H_{17}O_2^-$ (*m/z* 145.1232), before H/D exchange, with $C_8H_{16}D_1O_2^-$ (*m/z* 146.1295) and $C_8H_{15}D_2O_2^-$ (*m/z* 147.1358) obtained after one and two H/D exchanges, respectively. The JSR sample at 600 K was used for the H/D exchange.

Dihydroperoxides ($C_7H_{16}O_4$ and $C_8H_{18}O_4$) may also be produced during low-temperature oxidation of the fuel. They can result from H-atom abstraction from ROOH species, followed by O_2 addition and reaction with the hydroperoxy radical: ROOH + X$^\bullet$ → $^\bullet$ROOH + XH; $^\bullet$ROOH + O_2 → $^\bullet$OOROOH; $^\bullet$OOROOH + $HO_2^\bullet$ → $R(OOH)_2$ + O_2. $C_7H_{15}O_4^-$ (*m/z* 163.0977) signal corresponding to $C_7H_{16}O_4$ was detected in JSR and motored engine samples, as shown in Figure 4a. However, a very weak chromatographic signal corresponding to $C_8H_{18}O_4$ ($C_8H_{17}O_4^-$, *m/z* 177.1133) was detected only in the JSR sample at 600 K. Therefore, no profile is presented. In RCM experiments, $C_7H_{16}O_4$ and $C_8H_{18}O_4$ were not detected. JSR's experimental signal profile corresponding to $C_7H_{15}O_4^-$ is shown in Figure 4b. One can see that these intermediates reach a maximum signal at 600 K. The presence of two OOH chemical groups such as in dihydroperoxides ($C_7H_{16}O_4$), have been characterized by H/D exchange as shown in Supporting Information, Figure S1. The analyses revealed the presence of $C_7H_{14}D_2O_4$ using negative APCI ($C_7H_{13}D_2O_4^-$ with *m/z* 165.1099). Note that since no more than two H/D exchanges were detected, this should imply that tetraols (four OH functions) with the same formula were not observed in the samples.

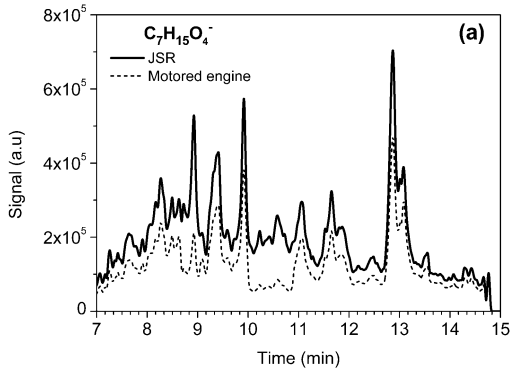

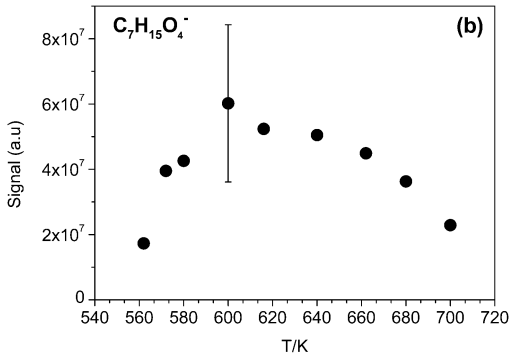

Figure 4. (a) Comparison between $C_7H_{16}O_4$ chromatogram obtained using UHPLC C_{18} negative APCI HRMS analyses ($C_7H_{15}O_4^-$, *m/z* 163.0977) for the oxidation of a PRF 50 in JSR (600 K) and motored engine experiments. (b) Experimental UHPLC signal for $C_7H_{15}O_4^-$ formed in a JSR.

3.2. Olefinic hydroperoxides, olefinic diols ($C_7H_{14}O_2$, and $C_8H_{16}O_2$), and olefinic di-hydroperoxides ($C_7H_{14}O_4$, and $C_8H_{16}O_4$). Olefinic hydroperoxides can be produced during the low-temperature oxidation of fuels: RH + X$^\bullet$→ R$^\bullet$ + XH; R$^\bullet$ + O_2 → ROO$^\bullet$; ROO$^\bullet$ (H-shift) →$^\bullet$QOOH; $^\bullet$QOOH + O_2→$^\bullet$OOQOOH; $^\bullet$OOQOOH (H-shift) → $^\bullet$Q'$(OOH)_2$→ Q'OOH + $HO_2^\bullet$. Signals corresponding to $C_7H_{14}O_2$ and $C_8H_{16}O_2$ were detected using UHPLC coupled to negative APCI-HRMS ($C_7H_{13}O_2^-$, *m/z* 129.0920, and $C_8H_{15}O_2^-$, *m/z* 143.1075) as shown in Figure 5a,b. We observed that signals corresponding to C7-olefinic hydroperoxides obtained for motored engine and JSR samples are consistent. However, some $C_8H_{15}O_2^-$ isomers are less present in motored engine than in JSR (e.g., Rt 16.05 and 16.28 min). Unfortunately, because RCM sample are less concentrated, some chromatographic peaks are almost absent. The analysis of an heptanoic acid standard (from Sigma-Aldrich®), an isomer of $C_7H_{14}O_2$ unsaturated hydroperoxides, was used to identify it at a retention time of 15.88 min.

Figure 5c shows the variation of $C_7H_{13}O_2^-$ and $C_8H_{15}O_2^-$ UHPLC-HRMS signals as function of JSR temperature. One can see that the sum of $C_7H_{13}O_2^-$ peaks area is higher (maximum at $9.22x10^9$) than that of $C_8H_{15}O_2^-$ (maximum at $1.51x10^9$). Hence, one can deduce that the olefinic hydroperoxides from *n*-heptane are likely more abundant than those from iso-octane.

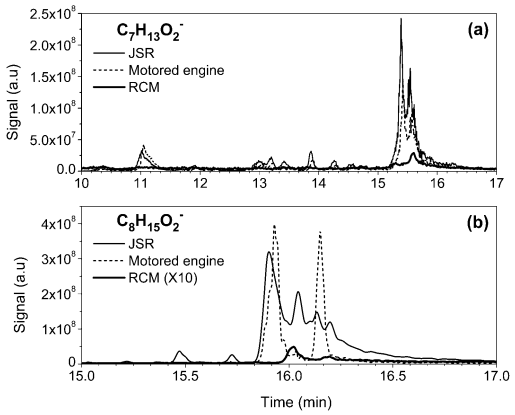

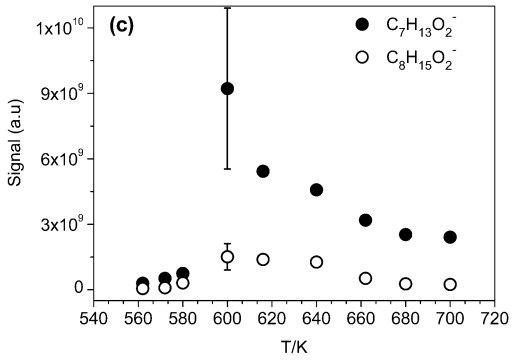

Figure 5. Comparison between chromatograms of (a) $C_7H_{13}O_2^-$ and (b) $C_8H_{15}O_2^-$ obtained with JSR (600 K), RCM, and motored engine samples. (c) UHPLC signal profiles for $C_7H_{13}O_2^-$ and $C_8H_{15}O_2^-$ obtained in JSR experiments (10 atm, 560-700 K).

Olefinic dihydroperoxides can be formed from olefinic hydroperoxides: Q"OOH + X$^{\bullet}$→ $^{\bullet}$Q"OOH+ XH; $^{\bullet}$Q"OOH+ O_2→ $^{\bullet}$OOQ"OOH; $^{\bullet}$OOQ"OOH+ HO_2→Q"$(OOH)_2$. In the case of the PRF 50 mixture, signals corresponding to $C_7H_{14}O_4$ and $C_8H_{16}O_4$ were detected using negative mode APCI ($C_7H_{13}O_4^-$, *m/z* 161.0818, and $C_8H_{15}O_4^-$, *m/z* 175.0977). Chromatograms are presented in Figure 6a,b. One can see that, despite a difference in intensities, $C_7H_{13}O_4^-$ and $C_8H_{15}O_4^-$ chromatograms from JSR and motored engine samples are consistent. One should note that these ions were detected in the too diluted RCM sample. $C_7H_{13}O_4^-$ and $C_8H_{15}O_4^-$ UHPLC signal profiles as a function of the JSR temperature are plotted (Figure 6c). It can be seen that the signal of $C_8H_{15}O_4^-$ two times higher than that of $C_7H_{13}O_4^-$, and both peak at 600K, as the other peroxidic intermediates probed in the JSR samples.

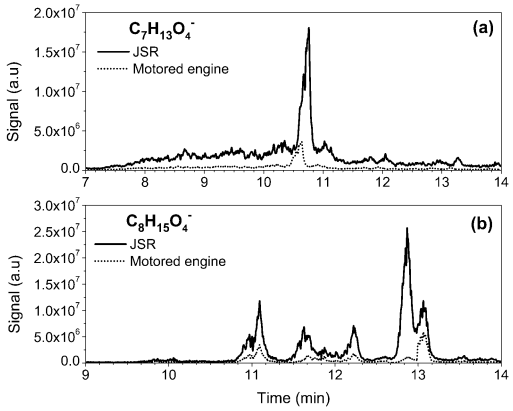

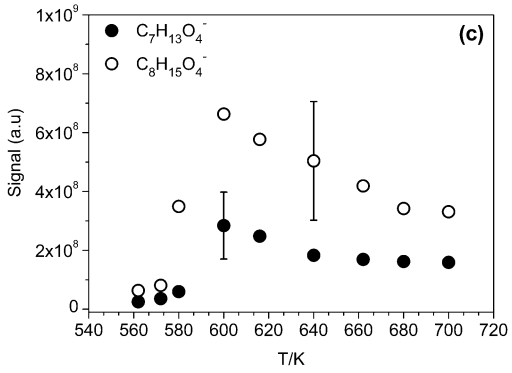

Figure 6. Comparison between UHPLC negative APCI HRMS signal of (a) $C_7H_{13}O_4^-$ and (b) $C_8H_{15}O_4^-$ corresponding to $C_7H_{14}O_4$ and $C_8H_{16}O_4$ olefinic dihydroperoxides formed during the low-temperature oxidation of PRF 50 in JSR (600 K) and motored engine experiments. (c) UHPLC signals for $C_7H_{13}O_4^-$ and $C_8H_{15}O_4^-$ as function of JSR's temperature.

3.3. Cyclic ethers, ketones, and aldehydes ($C_7H_{14}O$, and $C_8H_{16}O$). Cyclic ethers (QO) can be formed under oxidation conditions: RH + X˙ → R˙ + XH; R˙ + O_2 → ROO˙ → ˙QOOH (H-shift); ˙QOOH → QO + ˙OH. Several studies highlighted the formation of C_7 and C_8 oxygenated heterocycles species during *n*-heptane and iso-octane oxidation in JSR, RCM, and motored engine[5, 29-33]. Their importance varies according to the experimental conditions. For example, 2-methyl-5-ethyl- tetrahydrofuran, 2-butyl-3-methyl-oxirane and 2-propyl-THF are predominant during *n*-heptane oxidation. 2,2,4,4-tetra-methyl-tetrahydrofuran, 2-tertbutyl-3-methyl-oxetane, and 2-isopropyl-3,3-dimethyl-oxetane are a formed during iso-octane oxidation[5, 29-33]. The formation pathways for 2-methyl-5-ethyl-THF and 2,2,4,4-tetramethyl-THF, are presented in Scheme 1. The formation pathways for other $C_7H_{14}O$ and $C_8H_{16}O$ oxygenated heterocycles, such as 2-methyl-4-propyl-oxetane, 2-butyl-3-methyl-oxirane, 2-propyl-THF, 2,4-dimethyl-oxetane, 2-tertbutyl-3-methyl-oxetane, 2-isopropyl-3,3-dimethyl-oxetane, are presented in Supporting Information, Scheme S1.

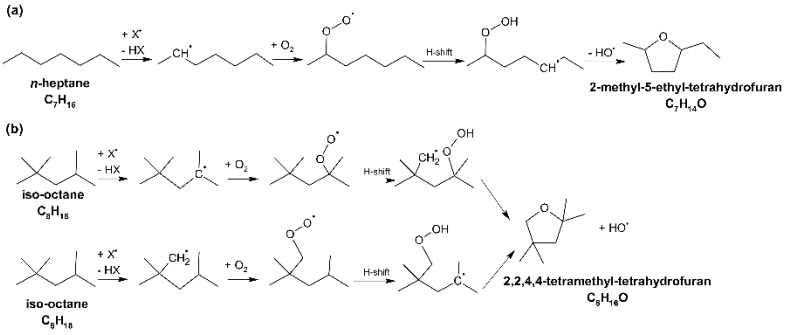

Scheme 1. Formation pathways for (a) 2-methyl-5-ethyl-THF and (b) for 2,2,4,4-tetramethyl-THF formed during the oxidation of *n*-heptane and iso-octane, respectively.

$C_7H_{14}O$ and $C_8H_{16}O$ are chemical formulae common to cyclic ethers and ketones/aldehydes (carbonyls) which can be formed during the oxidation of *n*-heptane and iso-octane, respectively. C_7 and

C_8 carbonyl compounds are formed from ˙QOOH. Scheme 2a,b shows possible formation pathways for 2-heptanone ($C_7H_{14}O$) and 2,2,4-trimethyl-pentan-3-one ($C_8H_{16}O$), respectively. Proposed formation pathways for the other $C_7H_{14}O$ and $C_8H_{16}O$ carbonyls, i.e., heptanal, 3 and 4-heptanone, 2,4,4-trimethyl-pentanal, and 2,2,4-trimethyl-pentanal, are presented in Supporting Information, Scheme S2. It is useful to note that, in addition to heptanones and heptanal, $C_7H_{14}O$ may also correspond to carbonyls (4,4-dimethyl-pentanal and 4,4-dimethyl-pentan-2-one) resulting from the decomposition iso-octane's KHPs ($C_8H_{16}O_3$), or from the decomposition of a RO˙ radical ($C_8H_{17}O$˙), as shown in Scheme 2c.

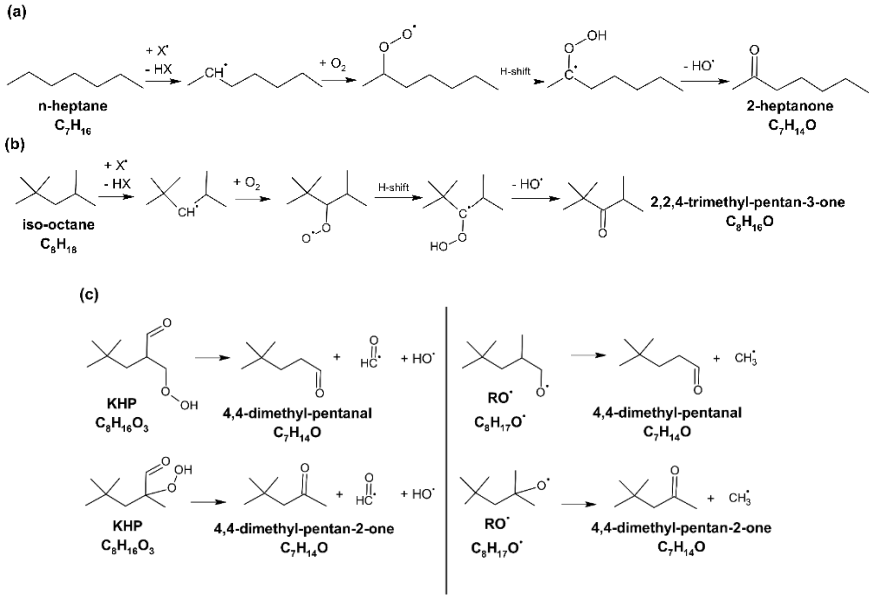

Scheme 2. Formation pathways of (a) 2-heptanone, (b) 2,2,4-trimethyl-pentan-3-one, and (c) 4,4-dimethyl-pentanal, and 4,4-dimethyl-pentan-2-one.

UHPLC/APCI(+/–)/HRMS analyses of $C_7H_{14}O$ and $C_8H_{16}O$ were performed ($C_7H_{15}O^+$ with *m/z* 115.1116, $C_7H_{13}O^-$ with *m/z* 113.0970, $C_8H_{17}O^+$ with *m/z* 129.1272, and $C_8H_{15}O^-$ with *m/z* 127.1127). Figure 7a,b show chromatograms for $C_7H_{15}O^+$ and $C_8H_{17}O^+$ ions detected by analyzing JSR (620 K), RCM, and motored engine samples. One can see that, despite a stronger signal obtained for the JSR samples, there is a good match between all the experimental data. Concerning $C_7H_{14}O$ compounds, UHPLC positive APCI analyses of standards (from Sigma-Aldrich®) showed the presence of 2-heptanone at a retention time (Rt) of 16,16 min. However, 3- and 4-heptanone were co-eluted (Rt = 16.19 min). 4.4-dimethyl-pentanal and heptanal were identified using negative APCI at Rt = 16.41 and 16.52 min, respectively (Supporting Information, Figure S2.). The others peaks (Rt ~ 15.50 to 16.09, and 16.33 min) correspond to $C_7H_{14}O$ cyclic ethers. Profiles of signals for heptanones, 4.4-dimethyl-pentanal, heptanal, and the sum of $C_7H_{14}O$ cyclic ethers formed in JSR, are presented in Figure 7c,d,e. The results show that all the $C_7H_{14}O$ ketones/aldehydes reach a maximum at 600 K, which corresponds to the maximum formation of KHPs[9]. Also, one can note that the signal for 4.4-dimethylpentanal is

higher ($8.86x10^7$) than that for heptanal ($2.50x10^7$). Based on Figure 7e, one can see that $C_7H_{14}O$ cyclic ethers reach a maximum at 700 K.

Concerning $C_8H_{16}O$, UHPLC analyses indicated the presence of co-eluted products (Rt ~ 16.19-16.73 min). Experimental data profiles are plotted in Figure 7f. One can see that signal reaches a first maximum at 600 K, which might correspond to the formation of carbonyls, then reaches a second maximum at ~700 K, which could correspond to cyclic ethers. These results confirm the co-elution of intermediates. Unfortunately, the non-availability of standards did not allow us to identify and distinguish between $C_8H_{16}O$ cyclic ethers and carbonyls.

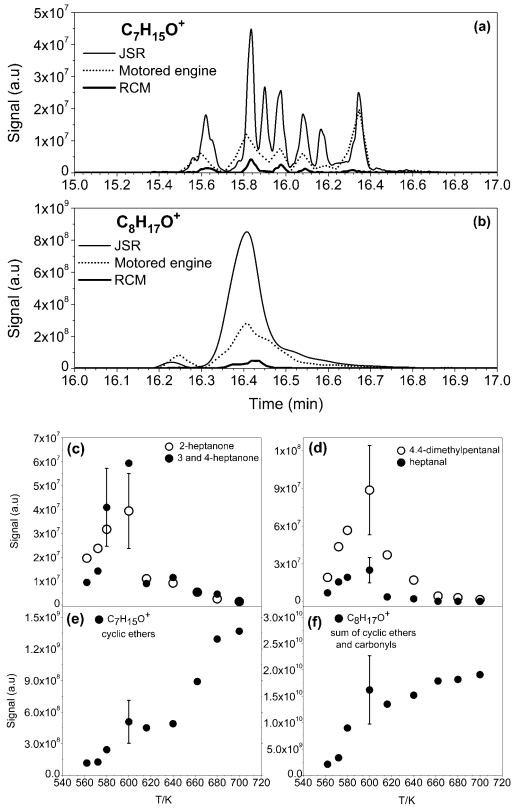

Figure 7. Comparison between UHPLC APCI(+)/HRMS signal of (a) $C_7H_{15}O^+$ and (b) $C_8H_{17}O^+$ corresponding to $C_7H_{14}O$ and $C_8H_{16}O$ cyclic ethers/carbonyls formed during the oxidation of PRF 50 in JSR (620 K), RCM, and motored engine. (c) Experimental UHPLC APCI(+)/HRMS signal profiles for 2-heptanone, and the sum of 3- and 4-heptanone. (d) Experimental UHPLC APCI(–) HRMS signal profiles for 4,4-dimethyl-pentanal and heptanal. (e) Experimental UHPLC APCI(+)/HRMS signal profiles for the sum of $C_7H_{14}O$ cyclic ethers. (f) Experimental UHPLC APCI(+)/HRMS signal profile for the sum of $C_8H_{16}O$ cyclic ethers/carbonyls formed in JSR samples (10 atm, 560-700 K).

3.4. Olefinic, di-olefinic, and tri-olefinic cyclic ethers/ketones/aldehydes ($C_7H_{12}O$, $C_8H_{14}O$, $C_7H_{10}O$, and C_7H_8O). In several experimental studies of PRFs oxidation, the presence of unsaturated

and di-unsaturated cyclic ethers/carbonyls has been reported[2, 31]. Cyclic ethers with one, two, or three double bonds can be produced through the following set of reactions:

$QO + X^{\bullet} \rightarrow {}^{\bullet}QO + XH$; ${}^{\bullet}QO + O_2 \rightarrow {}^{\bullet}OOQO \rightarrow HOOQ^{\bullet}O$ (H-shift) $\rightarrow Q^{'}O$ (olefinic cyclic ether) + $HO_2^{\bullet}$

$Q^{'}O + X^{\bullet} \rightarrow {}^{\bullet}Q^{'}O + XH$; ${}^{\bullet}Q^{'}O + O_2 \rightarrow {}^{\bullet}OOQ^{'}O \rightarrow HOO\,Q^{\bullet'}O$ (H-shift) $\rightarrow Q^{''}O$ (di-olefinic cyclic ether) + $HO_2^{\bullet}$

$Q^{''}O + X^{\bullet} \rightarrow Q^{\bullet''}O + XH$; $Q^{\bullet''}O + O_2 \rightarrow {}^{\bullet}OOQ^{''}O \rightarrow HOOQ^{\bullet''}O$ (H-shift) $\rightarrow Q^{'''}O$ (tri-olefinic cyclic ether) + $HO_2^{\bullet}$.

Scheme 3a,b, shows some examples of $C_7H_{12}O$ and $C_8H_{14}O$ olefinic cyclic ethers formed by decomposition of $C_7H_{14}O$ and $C_8H_{16}O$ cyclic ethers, respectively. Scheme 3c,d, shows the formation of some di-olefinic and tri-olefinic cyclic ethers, $C_7H_{10}O$ and C_7H_8O, respectively. Proposed formation pathways for other C_7-cyclic ethers with one, two or three unsaturation ($C_7H_{12}O$, $C_7H_{10}O$, and C_7H_8O), are presented in Supporting Information, Scheme S3.

One should note that for the branched $C_8H_{16}O$ cyclic ethers, the possibilities to form olefinic cyclic ethers are limited and it is not possible to form di and tri-olefinic oxygenated heterocycles ($C_8H_{12}O$ and $C_8H_{10}O$).

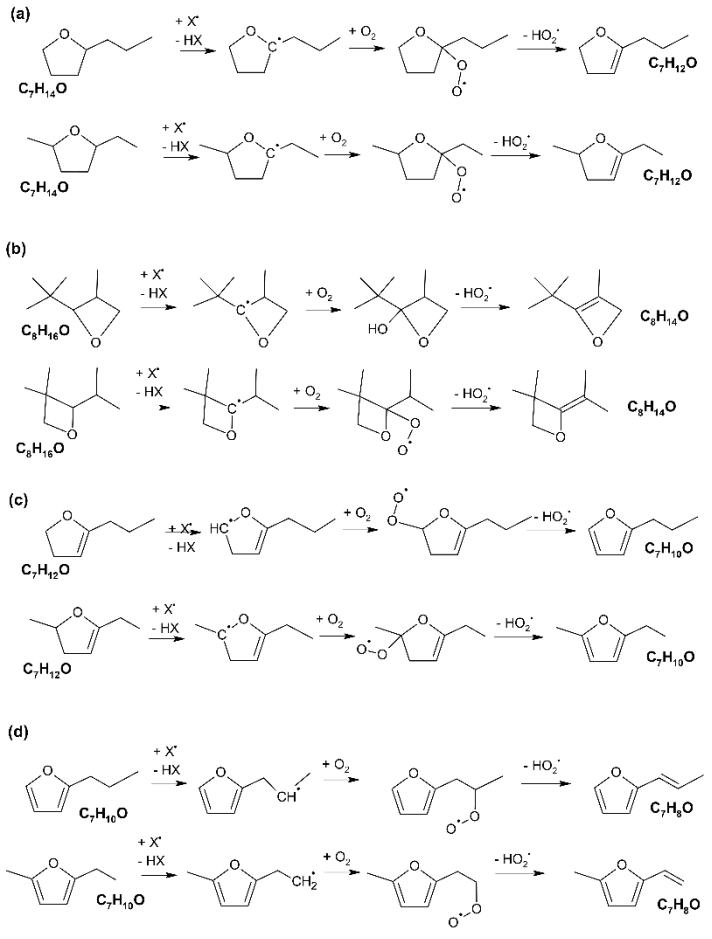

Scheme 3. Proposed formation pathways of some C_7 and C_8 unsaturated cyclic ethers through *n*-heptane and iso-octane oxidation. (a) $C_7H_{12}O$ and (b) $C_8H_{14}O$ olefinic cyclic ethers, (c) $C_7H_{10}O$ di-olefinic cyclic ethers, and (d) C_7H_8O tri-olefinic cyclic ethers.

In addition to cyclic ethers with one, two or three C-C double bonds, olefinic di- and tri-olefinic carbonyls, $C_7H_{12}O$, $C_8H_{14}O$, $C_7H_{10}O$, and C_7H_8O, respectively, can also be formed during the oxidation of *n*-heptane and iso-octane. Examples are presented in Scheme 4. Formation pathways of other olefinic, di- and tri-olefinic carbonyls are given in Supporting Information, Scheme S4. One should note that di- and tri-olefinic branched C_8-ketones/aldehydes ($C_8H_{12}O$, $C_8H_{10}O$) cannot be formed.

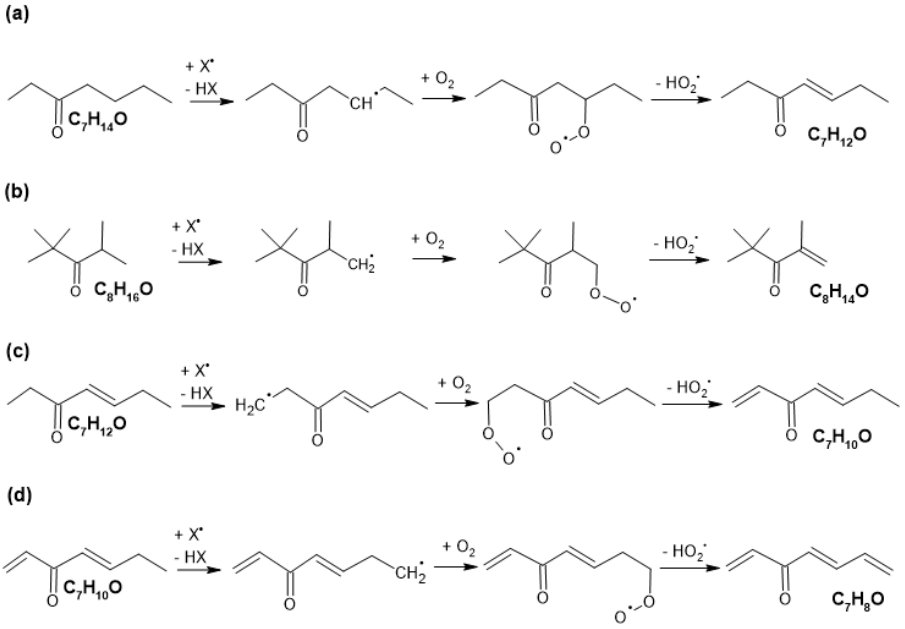

Scheme 4. Proposed formation pathways for some C_7 and C_8 olefinic ketones/aldehydes from *n*-heptane and iso-octane oxidation. (a) $C_7H_{12}O$ and (b) $C_8H_{14}O$ olefinic ketones/aldehydes, (c) $C_7H_{10}O$ di-olefinic ketones/aldehydes, and (d) C_7H_8O tri-olefinic carbonyls.

UHPLC/APCI(+)/HRMS analyses showed the presence of several $C_7H_{12}O$ ($C_7H_{13}O^+$, *m/z* 113.0958), $C_8H_{14}O$ ($C_8H_{15}O^+$, *m/z* 127.1115), $C_7H_{10}O$ ($C_7H_{11}O^+$, *m/z* 111.0802), and C_7H_8O ($C_7H_9O^+$, *m/z* 109.0646) isomers. As can be seen from Figure 8a-e, the majority of the chromatographic data are in good agreement. However, some species were not detected in RCM and motored engine experiments, for example in Figure 8a at Rt 13.03, 13.44, and 13.96 min, and in Figure 8b,c the peak at Rt 13.15 min, and in Figure 8d, peaks at 7-11 min and 11.90 min. Also, it was noted that $C_7H_9O^+$ species were not detected in the RCM sample.

Unsaturated cyclic ethers/ketones standards for $C_7H_{12}O$, $C_7H_{10}O$, C_7H_8O, and $C_8H_{14}O$ were not commercially available. Therefore, the distinction between the two chemical classes, olefinic cyclic ethers and olefinic carbonyls, might be possible only by plotting and comparing the profiles of each chromatographic peak present in Figure 8a-e. In Figure 8a, $C_7H_{12}O$ olefinic cyclic ethers were identified at Rt ~10 to 12.50 min, and Rt = 15.59 to 15.95 min. $C_7H_{12}O$ olefinic carbonyls were identified at Rt

~12.57 to 15.52 min and Rt = 16.13 to 16.85 min. Their respective profiles were plotted in Figure 8f. One can note that $C_7H_{12}O$ olefinic cyclic ethers reach a maximum at 662 K, and olefinic carbonyls at 600 K. This is consistent with the fact that olefinic ethers derive from cyclic ethers which reach a maximum concentration in the negative temperature region (>700 K)[9]. The profile presented in Figure 8g corresponds to the sum of all $C_8H_{15}O^+$ peaks (refer to Figure 8b,c, Rt ~ 11-17 min). Results show a maximum at 600 K, corresponding to maximum production of olefinic carbonyls. In Figure 8d, $C_7H_{10}O$ di-olefinic cyclic ethers were identified at Rt ~7.54 to 10.15 min, 10.56 to 11.45 min, 13.55 to 13.78 min, 15.18 and 15.93 min. $C_7H_{10}O$ di-olefinic ketones/aldehydes were identified at Rt 10.43, 11.63 to 13.51 min, 13.98 to 15.06 min, 15.48 min, and 15.98 to 16.97 min. Figure 8h illustrates the variation of their signals as a function of the JSR temperature. One can see that $C_7H_{10}O$ di-olefinic cyclic ethers reach a maximum at ~680 K, and di-olefinic carbonyls at 600 K. In Figure 8e, we can note a very good match between the chromatograms obtained for $C_7H_9O^+$ corresponding to C_7H_8O formed in JSR (660 K) and motored engine experiments. Tri-olefinic carbonyls were identified at Rt ~ 11.66 min. The other chromatographic peaks (Rt ~10.36 to 11.51 min and ~12.03 to 14.53 min) were attributed to tri-olefinic oxygenated heterocycles. Their UHPLC signal vs. JSR temperature are presented in Figure 8i. We observed a maximum formation of C_7H_8O tri-olefinic cyclic ethers at ~680 K, and C_7H_8O tri-olefinic carbonyls at ~ 600 K. On should note that the formation of $C_8H_{12}O$ and $C_8H_{10}O$, i.e., di- and tri-unsaturated cyclic ethers/ketones/aldehydes cannot occur.

In order to confirm the presence of a carbonyl function on $C_7H_{12}O$, $C_7H_{10}O$, C_7H_8O, and $C_8H_{14}O$ intermediates, DNPH derivatization was used ($C_7H_{12}O+C_6H_6O_4N_4 \rightarrow C_{13}H_{16}O_4N_4 + H_2O$, $C_7H_{10}O+C_6H_6O_4N_4 \rightarrow C_{13}H_{14}O_4N_4 + H_2O$, $C_7H_8O+C_6H_6O_4N_4 \rightarrow C_{13}H_{12}O_4N_4 + H_2O$ and $C_8H_{14}O+C_6H_6O_4N_4 \rightarrow C_{14}H_{18}O_4N_4 + H_2O$). Indeed, we could confirm the presence of olefinic carbonyl compounds. UHPLC/APCI(–)/HRMS analyses indicated the presence of several co-eluted peaks corresponding to DNPH-carbonyl derivatives ($C_{13}H_{15}O_4N_4^-$ with *m/z* 291.1098, $C_{13}H_{13}O_4N_4^-$ with *m/z* 289.0942, $C_{13}H_{11}O_4N_4^-$ with *m/z* 287.0771, and $C_{14}H_{17}O_4N_4^-$ with *m/z* 305.1255), see Supporting Information, Figure S3.

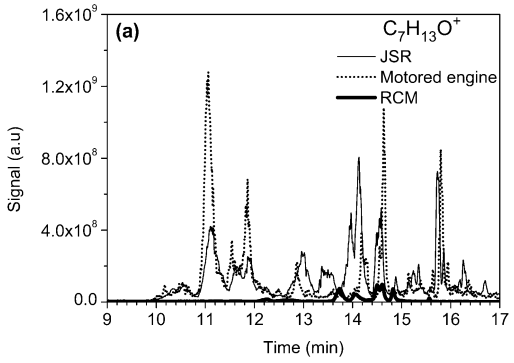

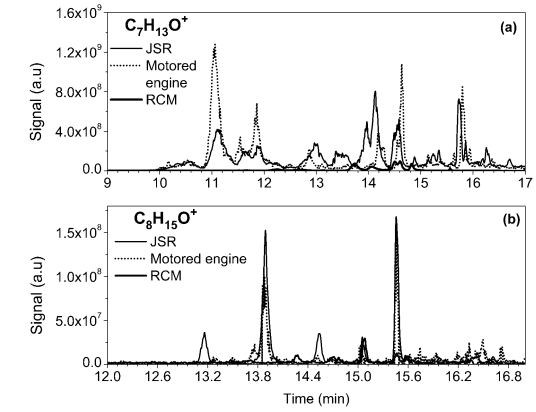
(a)
$C_7H_{13}O^+$
JSR
Motored engine
RCM
Signal (a.u)
(b)
$C_8H_{15}O^+$
JSR
Motored engine
RCM
Signal (a.u)
Time (min)

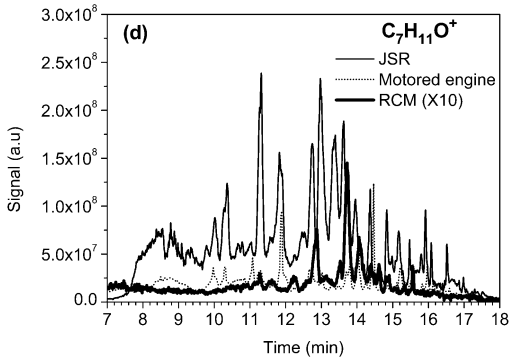
(d)
$C_7H_{11}O^+$
JSR
Motored engine
RCM (X10)
Signal (a.u)
Time (min)

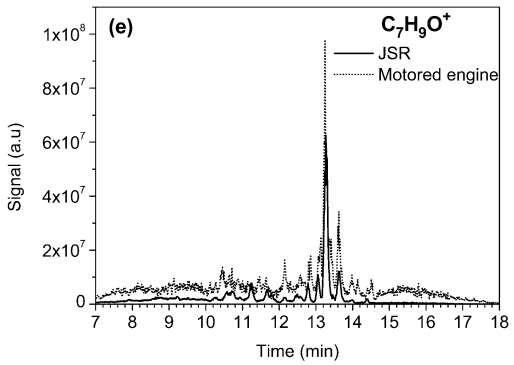
(e)
$C_7H_9O^+$
JSR
Motored engine
Signal (a.u)
Time (min)

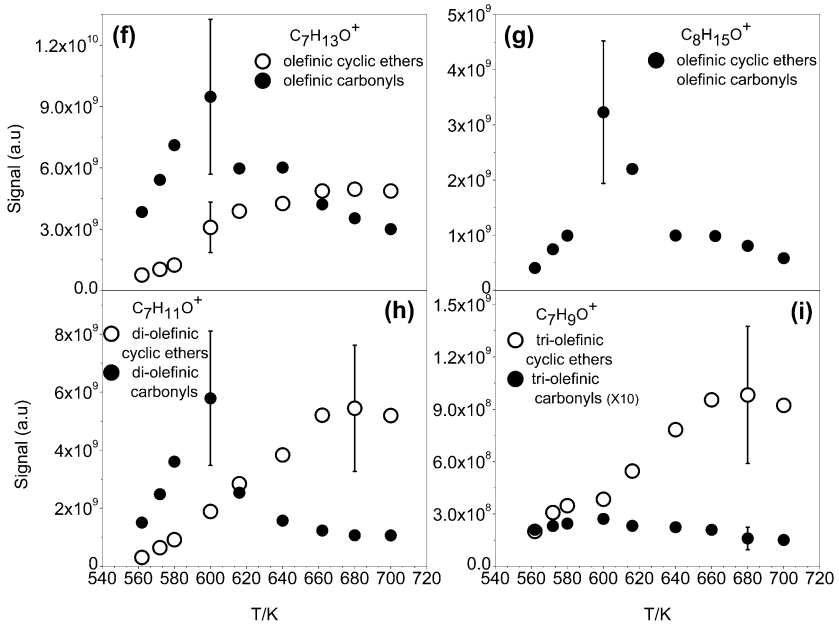
(f)
$C_7H_{13}O^+$
olefinic cyclic ethers
olefinic carbonyls
(g)
$C_8H_{15}O^+$
olefinic cyclic ethers
olefinic carbonyls
(h)
$C_7H_{11}O^+$
di-olefinic cyclic ethers
di-olefinic carbonyls
(i)
$C_7H_9O^+$
tri-olefinic cyclic ethers
tri-olefinic carbonyls (X10)
Signal (a.u)
T/K

Figure 8. Comparison between UHPLC/APCI(+)/HRMS signals for (a) $C_7H_{13}O^+$, (b) and (c) $C_8H_{15}O^+$, and (d) $C_7H_{11}O^+$, (e) $C_7H_9O^+$. UHPLC signal profiles vs. JSR temperature for (f) $C_7H_{13}O^+$ olefinic cyclic ethers and olefinic carbonyls, (g) sum of $C_8H_{15}O^+$ signals, (h) $C_7H_{11}O^+$ di-olefinic cyclic ethers and di-olefinic carbonyls, (i) $C_7H_9O^+$ tri-olefinic cyclic ether and tri-olefinic carbonyls.

3.5. Keto-hydroperoxides ($C_7H_{14}O_3$, $C_8H_{16}O_3$), olefinic keto-hydroperoxides ($C_7H_{12}O_3$, $C_8H_{14}O_3$), and di-olefinic KHPs ($C_7H_{10}O_3$). Keto-hydroperoxides are the most important cool flame intermediates for explaining low-temperature reactivity. They are formed from 2nd O_2 addition on fuel's radicals: RH + X$^\bullet$ → R$^\bullet$ + XH; R$^\bullet$ + O_2 → ROO$^\bullet$ → $^\bullet$QOOH (H-shift); $^\bullet$QOOH+ O_2 → $^\bullet$OOQOOH→ HOOQ$^\bullet$OOH (H-shift); → O=QOOH + HO$^\bullet$. Several studies have demonstrated the formation of KHPs during the low-temperature oxidation of *n*-heptane.[2, 25, 28, 31] As presented previously[9], KHPs ($C_7H_{14}O_3$ and $C_8H_{16}O_3$) are formed during the low-temperature oxidation of PRF 50 in JSR (φ= 0.5, 10 atm, 560-700 K) and RCM (φ= 0.5, 20 bar, 620 K) experiments. In the present study, we choose to compare their formation under JSR, RCM, and motored engine conditions. UHPLC/APCI(+)/HRMS analyses of $C_7H_{14}O_3$ and $C_8H_{16}O_3$ were performed. They showed the presence of several isomers ($C_7H_{15}O_3^+$ with *m/z* 147.1015, and $C_8H_{17}O_3^+$ with *m/z* 161.1170). As shown in Figure 9, there is a good agreement between UHPLC signals obtained for JSR and motored engine samples, whereas signals from the RCM sample are very weak. Only species eluted at Rt ~13.72 and 14.59 min (Figure 9a), match those of JSR and motored engine data. Signals recorded versus JSR temperature have been presented previously[9], showing a maximum formation at 600 K.

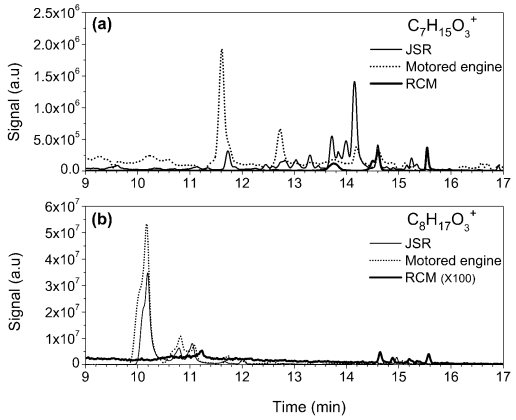

Figure 9. Comparison of UHPLC/APCI(+)/HRMS signals for (a) $C_7H_{15}O_3^+$ and (b) $C_8H_{17}O_3^+$ obtained by analyzing JSR, RCM, and motored engine samples.

Olefinic and di-olefinic KHPs ($C_7H_{12}O_3$, $C_8H_{14}O_3$, and $C_7H_{10}O_3$, respectively) can be formed during the low-temperature oxidation of a *n*-heptane/iso-octane mixture.[2] Some examples of possible formation pathways are presented in Scheme 5. The formation of branched $C_8H_{12}O_3$ di-unsaturated KHPs from iso-octane is not possible because there is no available hydrogen atom to abstract from olefinic KHPs

($C_8H_{14}O_3$) to form a double bond. Note that, $C_7H_{10}O_3$ and $C_8H_{12}O_3$ chemical formula also correspond to triketones. The analysis of the formation of these species is presented Section 3.7.

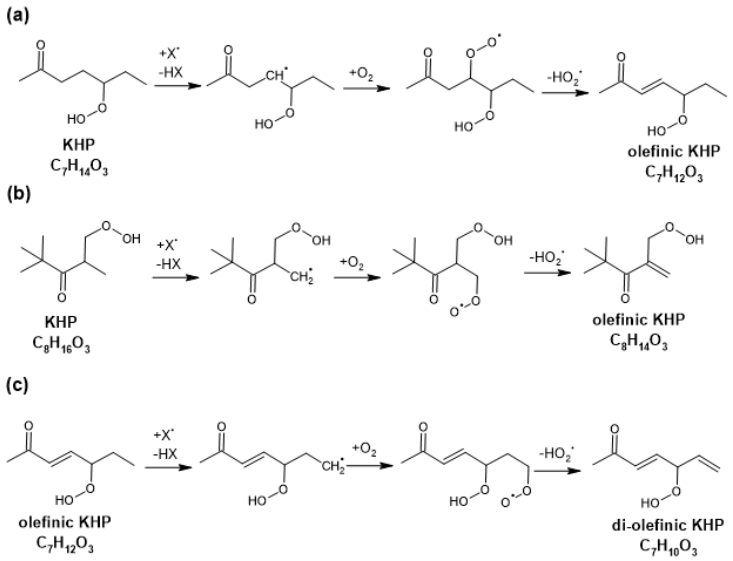

Scheme 5. Proposed formation pathways for (a) $C_7H_{12}O_3$, (b) $C_8H_{14}O_3$ olefinic KHPs, and (c) $C_7H_{10}O_3$ di-olefinic KHPs.

UHPLC coupled to APCI(+)/HRMS analyses, confirmed the presence of several $C_7H_{12}O_3$ and $C_8H_{14}O_3$ isomers ($C_7H_{13}O_3^+$ with *m/z* 145.0858, and $C_8H_{15}O_3^+$ with *m/z* 159.1015). In Figure 10a, b, we compare JSR (600 K) and motored engine chromatographic data. The results indicated that excepted for some minor peaks from the motored engine sample, e.g., peaks at Rt 8.91 and 11.08 min (Figure 10a), and peak at Rt 11.13 min (Figure 10b), JSR and motored engine experiments seem produce the same $C_7H_{12}O_3$ and $C_8H_{14}O_3$ oxidation intermediates. One should note that $C_7H_{13}O_3^+$ and $C_8H_{15}O_3^+$ were not detected in RCM sample.

In order to confirm that $C_7H_{12}O_3$ correspond to olefinic KHPs, MS/MS analyses were performed. The presence of several specific fragments confirmed the presence of a double bond (C=C), a C=O and an OOH functions. For example, the $C_4H_5O^+$ fragment indicated the presence of a carbonyl function and one unsaturation in a C_4-carbon chain. Fragments identification is presented in Supporting Information, Table S1.

Signal profiles obtained by UHPLC positive APCI/HRMS for $C_7H_{13}O_3^+$ and $C_8H_{15}O_3^+$, corresponding to $C_7H_{12}O_3$ and $C_8H_{14}O_3$ olefinic KHPs, are plotted in Figure 10c. One can note that species reach a maximum at 600 K. It was observed that the $C_8H_{15}O_3^+$signal is higher than that of $C_7H_{13}O_3^+$, which indicate that C_8-olefinic KHPs formation is favored.

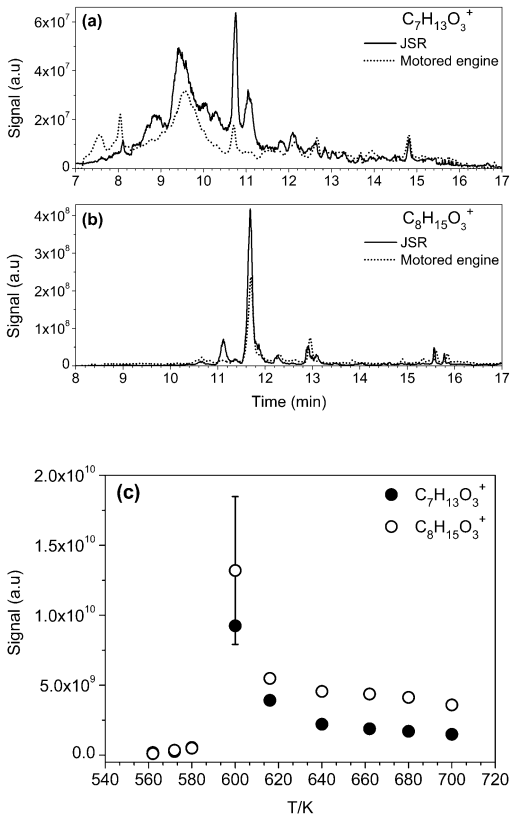

Figure 10. Comparison between UHPLC APCI(+)/HRMS analyses of (a) $C_7H_{11}O_3^+$ and (b) $C_8H_{15}O_3^+$, formed in JSR (600 K) and motored engine. (c) UHPLC signal vs. JSR temperature for $C_7H_{11}O_3^+$ and $C_8H_{13}O_3^+$.

3.6. Diketones ($C_7H_{12}O_2$, $C_8H_{14}O_2$), olefinic diketones ($C_7H_{10}O_2$, $C_8H_{12}O_2$), and di-olefinic diketones ($C_7H_8O_2$). As indicated previously[9], diketones formed during the low-temperature oxidation of *n*-heptane and iso-octane can be produced via multiple reaction pathways, e.g., decomposition of KHPs: O=QOOH + X$^\bullet$ → O=Q=O + HX + HO$^\bullet$. These diketones ($C_7H_{12}O_2$ and $C_8H_{14}O_2$) can decompose and form olefinic diketones ($C_7H_{10}O_2$ and $C_8H_{12}O_2$), which in turn can form di-olefinic diketones ($C_7H_8O_2$), as follow:

O=Q=O + X$^\bullet$ → Q$^\bullet$(=O)$_2$+ XH; Q$^\bullet$(=O)$_2$ + O_2 → $^\bullet$OOQ(=O)$_2$ → HOOQ$^\bullet$(=O)$_2$ (H-shift) → Q$^{'}$(=O)$_2$+ $HO_2^\bullet$.

Q$^{'}$(=O)$_2$ + X$^\bullet$→ Q$^{\bullet'}$(=O)$_2$ + XH; Q$^{\bullet'}$(=O)$_2$ + O_2 → $^\bullet$OOQ$^{'}$(=O)$_2$ → HOOQ$^{\bullet'}$(=O)$_2$ (H-shift) → Q$^{''}$(=O)$_2$ + $HO_2^\bullet$.

Thanks to the use of UHPLC coupled to positive APCI and HRMS, signals of $C_7H_{13}O_2^+$ (*m/z* 129.0908), $C_8H_{15}O_2^+$ (*m/z* 143.1065), $C_7H_{11}O_2^+$ (*m/z* 127.0752), $C_8H_{13}O_2^+$ (*m/z* 141.0908), and $C_7H_9O_2^+$ (*m/z* 125.0595), were detected in JSR, RCM, and motored engine samples. The corresponding chromatograms are presented in Figure 11a-e. From Figure 11a,b, one can see that more $C_7H_{13}O_2^+$ and $C_8H_{15}O_2^+$ species were detected in the JSR sample (600 K). For example, C_7-diketones isomers having retention times 12.45, 12.75, and 15.33 min (Figure 11a) are not present in the motored engine and RCM

data. This could be due to the weak formation of the KHPs ($C_7H_{14}O_3$) precursors under these experimental conditions. Also, only the $C_8H_{15}O_2^+$ isomer at 15.42 min (Figure 11b) is present in RCM data. Concerning Figure 11c,d, we note a very good match between $C_7H_{11}O_2^+$ and $C_8H_{13}O_2^+$, corresponding to olefinic diketones formed in JSR (600K) and motored engine experiments. In Figure 11e, one can see that similar $C_7H_9O_2^+$ isomers are present in both JSR and motored engine samples. However, $C_7H_{10}O_2$, $C_8H_{12}O_2$, and $C_7H_8O_2$ species, were not detected in less concentrated RCM sample. UHPLC signal profiles vs. JSR temperature for $C_7H_{11}O_2^+$, $C_8H_{13}O_2^+$, and $C_7H_9O_2^+$ are plotted in Figure 11f. There, one can see that C_7-olefinic diketones are more abundant than C_8-olefinic diketones and C_7-di-olefinic diketones. Both reach a maximum production at 600 K. UHPLC profiles for diketones ($C_7H_{12}O_2$, and $C_8H_{14}O_2$) have already been presented previously[9].

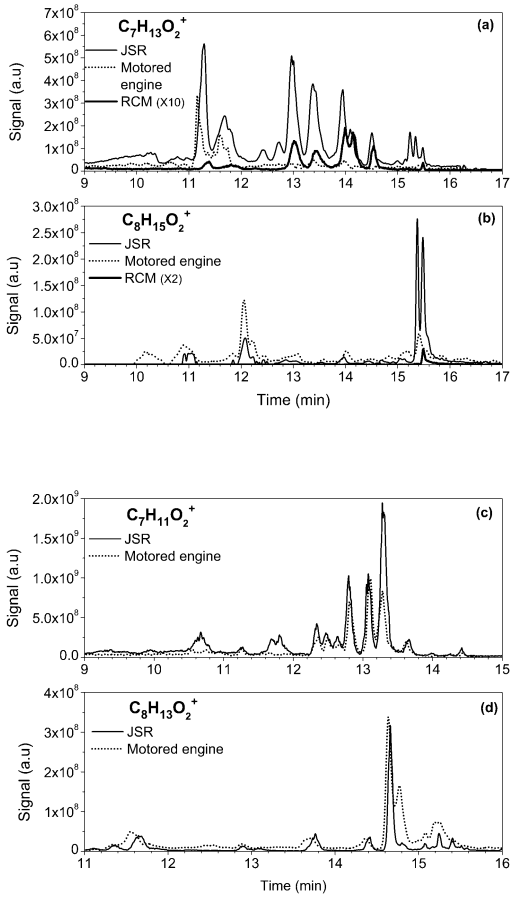

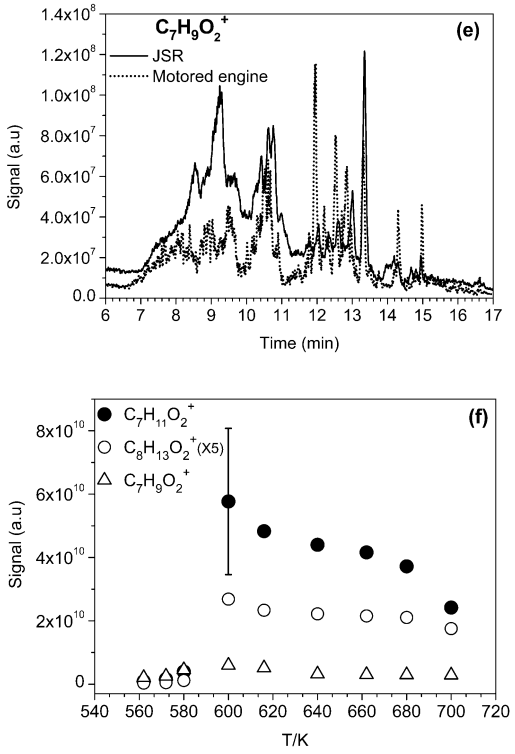

Figure 11. Comparison between UHPLC positive APCI/HRMS analyses of (a) $C_7H_{13}O_2^+$ (b) $C_8H_{15}O_2^+$, (c) $C_7H_{11}O_2^+$, (d) $C_8H_{13}O_2^+$, and (e) $C_7H_9O_2^+$, corresponding to diketones ($C_7H_{12}O_2$, $C_8H_{14}O_2$), olefinic diketones ($C_7H_{10}O_2$, $C_8H_{12}O_2$), and di-olefinic diketones ($C_7H_8O_2$) formed during the low-temperature oxidation of PRF 50 under JSR (10 atm, 600 K), RCM, and motored engine conditions. (f) UHPLC signal profiles vs. JSR temperature of $C_7H_{11}O_2^+$, $C_8H_{13}O_2^+$, and $C_7H_9O_2^+$.

3.7. Triketones ($C_7H_{10}O_3$, $C_8H_{12}O_3$). Species with three carbonyl groups, known as triketones ($C_7H_{10}O_3$ and $C_8H_{12}O_3$), can be formed from the decomposition of diketo-hydroperoxide intermediates ($C_7H_{12}O_4$ and $C_8H_{14}O_4$): $(HOO)P(=O)_2 + X^{\bullet} \rightarrow (HOO)P^{\bullet}(=O)_2 + HX \rightarrow P(=O)_3 + {}^{\bullet}OH$. Triketones, such as 2,4,6-heptanetrione, have been identified during *n*-heptane oxidation under motored engine conditions.[27] Signals corresponding to $C_7H_{10}O_3$ and $C_8H_{12}O_3$ were detected by UHPLC coupled to APCI(+/–)/HRMS ($C_7H_{11}O_3^+$ with *m/z* 143.0700, $C_7H_9O_3^-$ with *m/z* 141.0556, $C_8H_{13}O_3^+$ with *m/z* 157.0857, and $C_8H_{11}O_3^-$ with *m/z* 155.0713), as shown in Supporting Information, Figure S4. Results showed that $C_7H_{10}O_3$ and $C_8H_{12}O_3$ are better ionized in positive mode APCI. Therefore, UHPLC/APCI(+) results for $C_7H_{11}O_3^+$ and $C_8H_{13}O_3^+$ obtained for JSR samples were compared to those obtained under motored engine conditions (Figure 12a,b). One can see from Figure 12a, that similar $C_7H_{11}O_3^+$ chromatograms were obtained, although peaks at Rt = 9.32, and 14.65 min are more intense for the JSR sample. However, for $C_8H_{13}O_3^+$ isomers we observed a very good match between chromatograms obtained with JSR and motored engine samples (Figure 12b).

As mentioned previously, in the case of *n*-heptane, $C_7H_{10}O_3$ may correspond to triketones, but also to di-olefinic KHPs (Scheme 5c). However, for iso-octane, $C_8H_{12}O_3$ species may only correspond to triketones, but not to di-olefinic KHPs. This is due to the lack of available sites in $C_8H_{14}O_3$ olefinic KHPs to form a double bond. In order to distinguish between triketones and di-olefinic KHPs corresponding to $C_7H_{10}O_3$, MS/MS analyses were performed. The fragmentation of $C_7H_{11}O_3^+$ isomers, eluted at different retention times (Rt 9.25, 10.77, and 10.98 min of Figure 12a), gave similar fragments, even if they had different relative abundance. This indicates a co-elution of triketones and di-olefinic KHPs isomers. Moreover, some fragments are common to both isomers, e.g., $C_3H_5O^+$ (*m/z* 57.0335), and $C_5H_7^+$ (*m/z* 67.0541). Representative fragments of di-olefinic KHPs were identified, e.g., $C_4H_7^+$ (*m/z* 55.0543), $C_4H_5O^+$ (*m/z* 69.0334), and $C_5H_7O^+$ (*m/z* 83.0490). Those of triketones were $C_4H_7O^+$ (*m/z* 71.0490), $C_4H_5O_2^+$ (*m/z* 85.0282), and $C_5H_7O_2^+$ (*m/z* 99.0439). Further fragments identification is presented in Supporting Information, Table S2.

$C_8H_{12}O_3$ may correspond to triketones formed during the low-temperature oxidation of iso-octane. MS/MS analyses showed the presence of fragments corresponding to triketones, e.g., $C_4H_7O^+$ (*m/z* 71.0490), $C_4H_5O_2^+$ (*m/z* 85.0283), $C_5H_7O_2^+$ (*m/z* 99.0439), and $C_7H_{11}O_2^+$ (*m/z* 127.0752). Fragments identification is presented in Supporting Information, Table S3. $C_7H_{11}O_3^+$ and $C_8H_{13}O_3^+$ UHPLC signals obtained as a function of JSR's temperature are presented in Figure 12c. Here, we considered that the $C_8H_{13}O_3^+$ profile corresponds to triketones only. However, the $C_7H_{11}O_3^+$ profile, corresponds to the sum of triketones and di-olefinic KHPs. The results indicate that both $C_7H_{11}O_3^+$ and $C_8H_{13}O_3^+$ reach a maximum at 600 K, which corresponds to temperature where KHPs reach their maximum concentration.

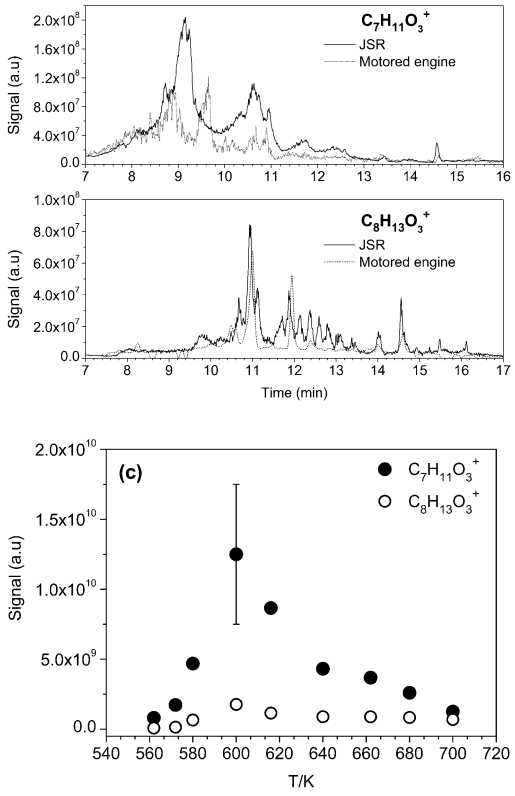

Figure 12. Comparison between UHPLC positive APCI chromatograms of (a) $C_7H_{11}O_3^+$ and (b) $C_8H_{13}O_3^+$. (c) UHPLC signals vs. JSR temperature of $C_7H_{11}O_3^+$ (*m/z* 143.0700) and $C_8H_{13}O_3^+$ (*m/z* 157.0857).

3.8. Highly oxygenated molecules: keto-dihydroperoxides ($C_7H_{14}O_5$, and $C_8H_{16}O_5$) and diketo-hydroperoxides ($C_7H_{12}O_4$, $C_8H_{14}O_4$). Due to the minor formation and the instability of highly oxygenated molecules (HOMs) such as keto-dihydroperoxides and diketo-hydroperoxides, these intermediates are not highlighted in modeling and experimental studies.

Keto-dihydroperoxides result from third O_2 addition on fuel's radicals: RH + X$^{\bullet}$→ R$^{\bullet}$ + XH; R$^{\bullet}$ + O_2 → ROO$^{\bullet}$ → $^{\bullet}$QOOH (H-shift); $^{\bullet}$QOOH + O_2 →$^{\bullet}$OOQOOH → $(HOO)_2Q^{\bullet\bullet}$ (H-shift); $(HOO)_2Q^{\bullet\bullet}$ + O_2 →$^{\bullet}$OOQ'$(OOH)_2$ → $^{\bullet}P(OOH)_3$ (H-shift) → $(HOO)_2P{=}O$ + $^{\bullet}$OH. Samples obtained from JSR, RCM, and motored engine experiments were analyzed using UHPLC/HRMS. Signals corresponding to $C_7H_{14}O_5$ and $C_8H_{16}O_5$ were detected in negative APCI ($C_7H_{13}O_5^-$ with *m/z* 177.0770, and $C_8H_{15}O_5^-$ with *m/z* 191.0926). Figure 13a,b shows chromatograms for $C_7H_{13}O_5^-$ and $C_8H_{15}O_5^-$. It can be seen that several isomers are present in both JSR and motored engine samples. For example, in Figure 13a, peaks at Rt 12.81, 13.11, 13.31, and 13.95 min. Also, in Figure 13b, isomers are eluted at Rt 12.09, 12.48, 13.31, 14.84, 15.13, and 15.53 min. However, some isomers are either absent in the motored engine sample, or are present at very low level compared to what we measured in JSR samples, e.g., peaks at Rt 10.28, 10.86, 10.98, and 12.45 min of Figure 13a. Because RCM samples were less concentrated, no signal corresponding to $C_7H_{14}O_5$ and $C_8H_{16}O_5$ was detected. Figure 13c shows UHPLC-HRMS experimental profiles for $C_7H_{13}O_5^-$ and $C_8H_{15}O_5^-$ from JSR samples. We can note that keto-dihydroperoxides reach their maximum intensity at 600 K, as KHPs do. C_7-keto-dihydroperoxides signals are more intense than those of C_8-keto-dihydroperoxides which could be attributed to the lower availability of easily abstractable C-H groups in the C_8-intermediates. MS/MS analyses of $C_7H_{13}O_5^-$ ions were performed. The analyses confirmed the presence of keto-dihydroperoxides ($C_7H_{14}O_5$), as reported in our previous work.[9]

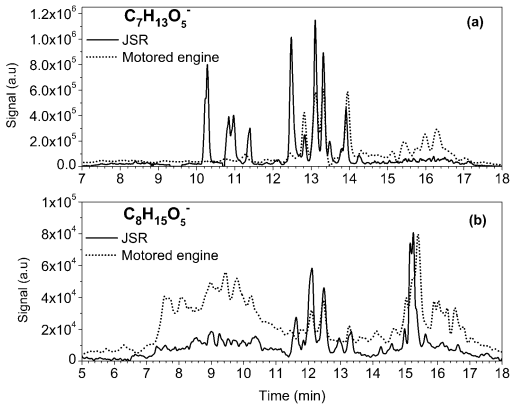

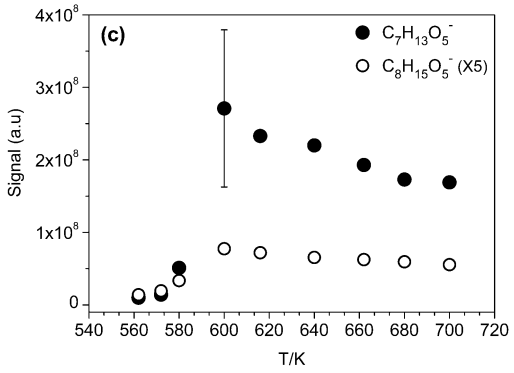

Figure 13. Comparison between (a) $C_7H_{13}O_5^-$ and (b) $C_8H_{15}O_5^-$ chromatograms obtained for JSR (600 K) and motored engine samples. (c) Experimental UHPLC APCI(–)/HRMS signal for $C_7H_{13}O_5^-$ and $C_8H_{15}O_5^-$ as function of JSR temperature.

Diketo-hydroperoxides can be formed through decomposition of keto-dihydroperoxides: $(HOO)_2P{=}O + X^{\bullet} \rightarrow (HOO)_2P^{\bullet}{=}O + HX \rightarrow HOOP(=O)_2 + {}^{\bullet}OH$. In the case of *n*-heptane and iso-octane, diketo-hydroperoxides correspond to $C_7H_{12}O_4$ and $C_8H_{14}O_4$, respectively. UHPLC coupled to APCI(+)/HRMS shown the presence of several $C_7H_{12}O_4$ and $C_8H_{14}O_4$ compounds ($C_7H_{13}O_4^+$ with *m/z* 161.0809 and $C_8H_{15}O_4^+$ with *m/z* 175.0964), as shown in Figure 14a,b. The analyses revealed that there are more isomers corresponding to C_8-diketo-hydroperoxides than C_7-diketo-hydroperoxides. The comparison between JSR and motored engine samples shows that $C_7H_{13}O_4^+$ formed in JSR and motored engine experiments, differ. For example, in Figure 14a, $C_7H_{13}O_4^+$ peaks at Rt ~9.42 to 9.96 min are more important in JSR than in motored engine sample. Conversely, peaks at Rt ~9.03, 9.59, 9.87, and 10.50 min, are more intense in motored engine sample. In Figure 14b, $C_8H_{15}O_4^+$ isomer at Rt = 13.03 min has a weaker peak in motored engine data. MS/MS analyses indicated the presence of several specific fragments corresponding to diketo-hydroperoxides ($C_7H_{12}O_4$), e.g., $C_4H_5O_2^+$ (*m/z* 85.0282), $C_5H_7O_2^+$ (*m/z* 99.0439), and $C_7H_{11}O_3^+$ (*m/z* 143.0701), which confirms that $C_7H_{13}O_4^+$ (*m/z* 161.0809) correspond to C_7-diketo-hydroperoxides formed during the low-temperature oxidation of *n*-heptane in the PRF 50 blend. Fragments identification is presented in Supporting Information, Table S4.

UHPLC signals vs. JSR's temperature of $C_7H_{13}O_4^+$ and $C_8H_{15}O_4^+$ are presented in Figure 14c. As well as for KHPs and keto-dihydroperoxides, a maximum signal was observed at 600 K. We can note that the signal of $C_8H_{15}O_4^+$ is slightly higher than that of $C_7H_{13}O_4^+$. This may explain the lower production of $C_8H_{16}O_5$ keto-dihydroperoxides which decompose to form diketo-hydroperoxides $C_8H_{14}O_4$.

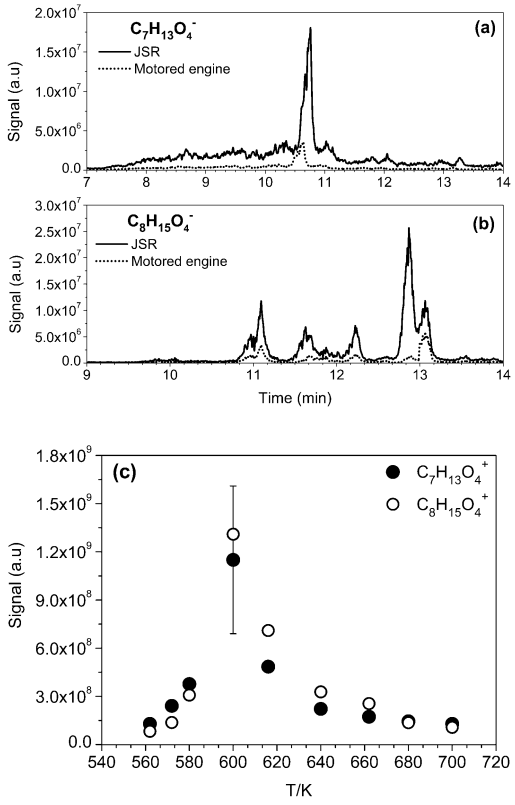

Figure 14. Comparison between (a) $C_7H_{13}O_4^+$ and (b) $C_8H_{15}O_4^+$ from UHPLC analyses of JSR (600 K) and motored engine samples. (c) Experimental UHPLC APCI(+)/HRMS signal versus JSR temperature for $C_7H_{13}O_4^+$ and $C_8H_{15}O_4^+$.

4. CONCLUSIONS

The low-temperature oxidation of *n*-heptane/iso-octane mixture (PRF 50) was studied in a single-cylinder motored engine modified to run in HCCI mode, a rapid compression machine, and a jet-stirred reactor. Identification of cool flame intermediates and products from the oxidation of a PRF 50 mixture, under JSR, RCM, and motored engine conditions, was achieved by combining UHPLC with APCI/ Orbitrap Q-Exactive™. For chromatographic analyses we used a reversed phase column and a water-acetonitrile mobile phase. For mass spectrometry analyses, positive ($[M+H]^+$) and negative ($[M-H]^-$) APCI modes were used. Oxidation products and intermediates were identified using tandem mass spectrometry. The presence of hydroperoxy groups were characterized by H/D exchange using deuterated water. The presence of carbonyl groups was verified through DNPH derivatization. UHPLC/APCI/ Orbitrap Q-Exactive™ analyses indicated the presence of several saturated and olefinic oxygenated intermediates. Besides cyclic ethers/ketones/aldehydes ($C_7H_{14}O$, $C_8H_{16}O$), ketohydroperoxides ($C_7H_{14}O_3$, $C_8H_{16}O_3$), diketones ($C_7H_{12}O_2$, $C_8H_{14}O_2$), and keto-dihydroperoxides ($C_7H_{14}O_5$, $C_8H_{16}O_5$), reported in our previous study on PRF 50 oxidation, a large set of newly detected or rarely considered low-temperature products were presented here: hydroperoxides and diols ($C_7H_{16}O_2$, $C_8H_{18}O_2$), olefinic hydroperoxides/diols ($C_7H_{14}O_2$, $C_8H_{16}O_2$), dihydroperoxides ($C_7H_{16}O_4$, $C_8H_{18}O_4$),

olefinic dihydroperoxides ($C_7H_{14}O_4$, $C_8H_{16}O_4$), olefinic cyclic ethers/carbonyls ($C_7H_{12}O$, $C_8H_{14}O$), di- and tri-olefinic cyclic ethers/ketones/aldehydes ($C_7H_{10}O$, C_7H_8O), olefinic ketohydroperoxides ($C_7H_{12}O_3$, $C_8H_{14}O_3$), di-olefinic ketohydroperoxides ($C_7H_{10}O_3$), triketones ($C_7H_{10}O_3$, $C_8H_{12}O_3$), olefinic diketones ($C_7H_{10}O_2$, $C_8H_{12}O_2$), di-olefinic diketones ($C_7H_8O_2$), and diketo-hydroperoxides ($C_7H_{12}O_4$, $C_8H_{14}O_4$). UHPLC-HRMS results obtained by analyzing motored engine, RCM, and JSR samples were compared, showing similar production for most of the species, despite the rather different physical operating conditions. This implies that in the three complementary experimental systems used for this study (motored engine, JSR, and RCM), the same chemical processes are involved in the fuel's low-temperature oxidation. They proceed through the initial formation of alkyl radicals which reacts with O_2 to form peroxy radicals. The further internal H-shifts and O_2 additions followed by decompositions are involved in the formation of the many products and intermediates observed in the three experimental systems considered in the present work. However, we noticed that the oxidation products presented different signal intensities, depending on the oxidation experiment. Indeed, chromatograms obtained for oxidation intermediates formed in RCM have significantly lower signal intensity than those corresponding to motored engine and JSR samples. Besides possible decomposition of chemical species on metallic surfaces (engine combustion chamber, stainless steel cylinders used for RCM sampling), the much smaller volume of gas sampled from RCM can explain the results. Although no quantification by UHPLC with APCI/ Orbitrap Q-Exactive™ could be performed, due to the lack of standards, the present results should be useful for future kinetic reaction mechanism developments.

■ ASSOCIATED CONTENT

Supporting Information: **Scheme S1.** Proposed formation pathways for (a) $C_7H_{14}O$ cyclic ethers (2-methyl-4-propyl-oxetane, 2-butyl-3-methyl-oxirane, 2-propyl-THF, and 2,4-dimethyl-oxetane), and (b) for $C_8H_{16}O$ cyclic ethers (2-tertbutyl-3-methyl-oxetane, 3-(1,1-dimethyl)-2,2-dimethyl-oxirane, and 2-isopropyl-3,3-dimethyl-oxetane), formed during the low-temperature oxidation of *n*-heptane and isooctane. **Scheme S2.** Proposed formation pathways for (a) $C_7H_{14}O$ carbonyls (heptanal, 3-heptanone, and 4-heptanone), and (b) for $C_8H_{16}O$ carbonyls (2,4,4-trimethyl-pentanal, and 2,2,4-trimethyl-pentanal), formed during the low-temperature oxidation of *n*-heptane and isooctane. **Scheme S3.** Proposed formation pathways for (a) $C_7H_{12}O$ olefinic cyclic ethers, (b) for $C_7H_{10}O$ di-olefinic cyclic ethers, and (c) C_7H_8O tri-olefinic cyclic ethers, formed during the low-temperature oxidation of *n*-heptane. **Scheme S4.** Proposed formation pathways for (a) $C_7H_{12}O$, and (b) for $C_8H_{14}O$ olefinic carbonyls, (c) $C_7H_{10}O$ di-olefinic carbonyls, and (d) C_7H_8O tri-olefinic carbonyls, formed during the low-temperature oxidation of *n*-heptane/iso-octane. **Figure. S1.** Comparison between UHPLC negative APCI HRMS signal of $C_7H_{15}O_4^-$ before H/D exchange and $C_7H_{13}D_2O_4^-$ formed after two H/D exchanges (JSR sample at 600 K). **Figure. S2.** Chromatogram showing UHPLC C_{18} negative APCI HRMS analysis of $C_7H_{13}O^-$ (*m/z* 113.0970) corresponding to $C_7H_{14}O$ intermediates formed during the low-temperature oxidation of PRF50 in a JSR (10 atm, 600 K). 4.4-dimethyl-pentanal and heptanal, were identified at 16.41 and 16.52 min, respectively. **Figure. S3**. Chromatograms showing UHPLC C_{18} negative APCI HRMS signals of (a) $C_{13}H_{15}O_4N_4^-$ (*m/z* 291.1098) corresponding to $C_7H_{12}O$ +DNPH, (b) $C_{13}H_{13}O_4N_4^-$ (*m/z* 289.0942) corresponding to $C_7H_{10}O$ +DNPH, (c) $C_{13}H_{11}O_4N_4^-$ (*m/z* 287.0771) corresponding to C_7H_8O +DNPH, and (d) $C_{14}H_{17}O_4N_4^-$ (*m/z* 305.1255) corresponding to $C_8H_{14}O$ +DNPH. Analyses of JSR sample at 600 K. **Table S1**. Identification of fragments corresponding to $C_7H_{12}O_3$ olefinic KHPs ($C_7H_{13}O_3^+$). Example of MSMS analysis of peak at 9.48 min (chromatogram of Figure 10a). **Figure. S4**.

Comparison between (a) $C_7H_{10}O_3$ and (b) $C_8H_{12}O_3$ UHPLC signals ($C_7H_{11}O_3^+$ with *m/z* 143.0700, $C_8H_{13}O_3^+$ with *m/z* 157.0857) and ($C_7H_9O_3^-$ with *m/z* 141.0556, $C_8H_{11}O_3^-$ with *m/z* 155.0713) using APCI (+/–). Analyses of JSR sample at 600K. **Table S2**. Identification of fragments corresponding to $C_7H_{10}O_3$ triketones and di-olefinic KHPs. Example of MSMS analysis of peak at 9.29 min ($C_7H_{11}O_3^+$ chromatogram of Figure 12a). **Table S3**. Identification of fragments corresponding to $C_8H_{12}O_3$ triketones ($C_8H_{13}O_3^+$). Example of MSMS analysis of peak at 11.07 min (refer to chromatogram of Figure 12b). **Table S4**. Identification of fragments corresponding to $C_7H_{12}O_4$ diketo-hydroperoxides ($C_7H_{13}O_4^+$). Example of MSMS analysis of peak at 9.45 min (refer to chromatogram of Figure 14a).

■ ACKNOWLEDGEMENTS

The authors gratefully acknowledge funding from the Labex CAPRYSSES (convention ANR-11-LABX-0006-01) and from the Region Centre Val de Loire, European Funds for Regional Development, and CPER (projects PROMESTOCK and APROPOR-E).

AUTHORS

Nesrine Belhadj − Institut de Combustion, Aérothermique, Réactivité et Environnement (ICARE), Centre National de la Recherche Scientifique (CNRS), 45071 Orléans, France; Université d'Orléans, 45067 Orléans, France ORCID: 0000-0002-5860-4144

Maxence Lailliau − Institut de Combustion, Aérothermique, Réactivité et Environnement (ICARE), Centre National de la Recherche Scientifique (CNRS), 45071 Orléans, France; Université d'Orléans, 45067 Orléans, France ORCID: 0000-0002-7758-3756

Zahraa Dbouk− Institut de Combustion, Aérothermique, Réactivité et Environnement (ICARE), Centre National de la Recherche Scientifique (CNRS), 45071 Orléans, France; Université d'Orléans, 45067 Orléans, France. ORCID: 0000-0002-8797-2990

Roland Benoit − Institut de Combustion, Aérothermique, Réactivité et Environnement (ICARE), Centre National de la Recherche Scientifique (CNRS), 45071 Orléans, France. ORCID: 0000-0001-8898-6131

Bruno Moreau – Laboratoire PRISME, Université d'Orléans, 45067 Orléans, France. ORCID: 0000-0002-6240-1710

Fabrice Foucher – Laboratoire PRISME, Université d'Orléans, 45067 Orléans, France. ORCID: 0000-0001-8469-8546

Philippe Dagaut − Institut de Combustion, Aérothermique, Réactivité et Environnement (ICARE), Centre National de la Recherche Scientifique (CNRS), 45071 Orléans, France. ORCID: 0000-0003-4825-3288

■ REFERENCES

(1) Dagaut, P.; Reuillon, M.; Cathonnet, M., High-Pressure Oxidation of Liquid Fuels from Low to High-Temperature .2. Mixtures of N-Heptane and Isooctane. *Combust. Sci. Technol.* **1994,** *103* (1-6), 315-336.

(2) Chen, B. J.; Ilies, D. B.; Hansen, N.; Pitsch, H.; Sarathy, S. M., Simultaneous production of ketohydroperoxides from low temperature oxidation of a gasoline primary reference fuel mixture. *Fuel* **2021,** *288*, 19737.

(3) Filipe, D. J.; Li, H. L.; Miller, D. L.; Cernansky, N. P., The Reactivity Behavior of n-Heptane and Isooctane Blends in a Motored Knock Research Engine, Technical Paper 920807. SAE International: 1992; pp 1-11.

(4) Leppard, W. R., The Autoignition Chemistries of Primary Reference Fuels, Olefin/Paraffin Binary Mixtures, and Non-Linear Octane Blending, Technical Paper 922325. SAE International: 1992; pp 1-23.

(5) Minetti, R.; Carlier, M.; Ribaucour, M.; Therssen, E.; Sochet, L. R., A rapid compression machine investigation of oxidation and auto-ignition of n-heptane: Measurements and modeling. *Combust. Flame* **1995,** *102* (3), 298-309.
(6) Minetti, R.; Carlier, M.; Ribaucour, M.; Therssen, E.; Sochet, L. R., Comparison of oxidation and autoignition of the two primary reference fuels by rapid compression. *Symposium (International) on Combustion* **1996,** *26* (1), 747-753.
(7) Karwat, D. M. A.; Wagnon, S. W.; Wooldridge, M. S.; Westbrook, C. K., Low-temperature speciation and chemical kinetic studies of n-heptane. *Combust. Flame* **2013,** *160* (12), 2693-2706.
(8) Tanaka, K.; Sugano, S.; Yokota, N.; Sakaida, S.; Konno, M.; Nakamura, H., Time-resolved Mid-infrared Measurements of Hydrogen Peroxide in the Low-temperature Oxidation of Iso-octane in a Rapid Compression Machine. *Combust. Sci. Technol.* **2020**, 1-17.
(9) Belhadj, N.; Benoit, R.; Dagaut, P.; Lailliau, M.; Moreau, B.; Foucher, F., Low-temperature oxidation of a gasoline surrogate: Experimental investigation in JSR and RCM using high-resolution mass spectrometry. *Combust. Flame* **2021,** *228*, 128-141.
(10) Malmberg, E. W.; Smith, M. L.; Bigler, J. E.; Bobbitt, J. A., A study of cool flames and associated reactions in an engine. *Symposium (International) on Combustion* **1955,** *5* (1), 385-392.
(11) Reda, A. A.; Schnelle-Kreis, J.; Orasche, J.; Abbaszade, G.; Lintelmann, J.; Arteaga-Salas, J. M.; Stengel, B.; Rabe, R.; Harndorf, H.; Sippula, O.; Streibel, T.; Zimmermann, R., Gas phase carbonyl compounds in ship emissions: Differences between diesel fuel and heavy fuel oil operation. *Atmos. Environ.* **2014,** *94*, 467-478.
(12) Rissanen, M. P.; Kurtén, T.; Sipilä, M.; Thornton, J. A.; Kangasluoma, J.; Sarnela, N.; Junninen, H.; Jørgensen, S.; Schallhart, S.; Kajos, M. K.; Taipale, R.; Springer, M.; Mentel, T. F.; Ruuskanen, T.; Petäjä, T.; Worsnop, D. R.; Kjaergaard, H. G.; Ehn, M., The Formation of Highly Oxidized Multifunctional Products in the Ozonolysis of Cyclohexene. *J. Am. Chem. Soc.* **2014,** *136* (44), 15596-15606.
(13) Li, R.; Wang, Z.; Xu, G., Study on Carbonyl Emissions of Diesel Engine Fueled with Biodiesel. *International Journal of Chemical Engineering* **2017,** *2017*, 1409495.
(14) Wang, Z.; Popolan-Vaida, D. M.; Chen, B.; Moshammer, K.; Mohamed, S. Y.; Wang, H.; Sioud, S.; Raji, M. A.; Kohse-Höinghaus, K.; Hansen, N.; Dagaut, P.; Leone, S. R.; Sarathy, S. M., Unraveling the structure and chemical mechanisms of highly oxygenated intermediates in oxidation of organic compounds. *Proceedings of the National Academy of Sciences* **2017,** *114* (50), 13102-13107.
(15) Kim, K. H.; Choi, B.; Park, S.; Kim, E.; Chiaramonti, D., Emission characteristics of compression ignition (CI) engine using diesel blended with hydrated butanol. *Fuel* **2019,** *257*, 116037.
(16) Benoit, R.; Belhadj, N.; Lailliau, M.; Dagaut, P., On the similarities and differences between the products of oxidation of hydrocarbons under simulated atmospheric conditions and cool flames. *Atmos. Chem. Phys.* **2021,** *21* (10), 7845-7862.
(17) Belhadj, N.; Benoit, R.; Dagaut, P.; Lailliau, M., Experimental characterization of n-heptane low-temperature oxidation products including keto-hydroperoxides and highly oxygenated organic molecules (HOMs). *Combust. Flame* **2021,** *224*, 83-93.
(18) Belhadj, N.; Benoit, R.; Dagaut, P.; Lailliau, M.; Serinyel, Z.; Dayma, G.; Khaled, F.; Moreau, B.; Foucher, F., Oxidation of di-n-butyl ether: Experimental characterization of low-temperature products in JSR and RCM. *Combust. Flame* **2020,** *222*, 133-144.
(19) Dagaut, P.; Cathonnet, M.; Rouan, J. P.; Foulatier, R.; Quilgars, A.; Boettner, J. C.; Gaillard, F.; James, H., A jet-stirred reactor for kinetic studies of homogeneous gas-phase reactions at pressures up to ten atmospheres (~ 1 MPa). *Journal of Physics E-Scientific Instruments* **1986,** *19* (3), 207-209.

(20) Dagaut, P.; Cathonnet, M.; Boettner, J. C.; Gaillard, F., Kinetic Modeling of Propane Oxidation. *Combust. Sci. Technol.* **1987,** *56* (1-3), 23-63.
(21) Dagaut, P.; Cathonnet, M.; Boettner, J. C.; Gaillard, F., Kinetic modeling of ethylene oxidation. *Combust. Flame* **1988,** *71* (3), 295-312.
(22) Mati, K.; Ristori, A.; Gail, S.; Pengloan, G.; Dagaut, P., The oxidation of a diesel fuel at 1-10 atm: Experimental study in a JSR and detailed chemical kinetic modeling. *Proc. Combust. Inst.* **2007,** *31* (2), 2939-2946.
(23) Cartlidge, J.; Tipper, C. F. H.; Bawn, C. E. H., The peroxides formed during hydrocarbon slow combustion and their role in the mechanism. *Proceedings of the Royal Society of London. Series A. Mathematical and Physical Sciences* **1961,** *261* (1306), 388-401.
(24) Sahetchian, K.; Rigny, R.; Blin, N., Evaluation of Hydroperoxide Concentrations During the Delay of Autoignition in an Experimental Four Stroke Engine: Comparison with Cool Flame Studies in a Flow System. *Combust. Sci. Technol.* **1988,** *60* (1-3), 117-124.
(25) Sahetchian, K. A.; Rigny, R.; Circan, S., Identification of the hydroperoxide formed by isomerization reactions during the oxidation of n-heptane in a reactor and CFR engine. *Combust. Flame* **1991,** *85* (3-4), 511-514.
(26) Blin-Simiand, N.; Rigny, R.; Viossat, V.; Circan, S.; Sahetchian, K., Autoignition of Hydrocarbon/Air Mixtures in a CFR Engine: Experimental and Modeling Study. *Combust. Sci. Technol.* **1993,** *88* (5-6), 329-348.
(27) Cartlidge, J.; Graham, J. K., The Initiation of the Pre-Flame Reaction of n-Heptane in a Motored Engine. *Combust. Sci. Technol.* **1995,** *109* (1-6), 141-164.
(28) Rodriguez, A.; Herbinet, O.; Meng, X. Z.; Fittschen, C.; Wang, Z. D.; Xing, L. L.; Zhang, L. D.; Battin-Leclerc, F., Hydroperoxide Measurements During Low-Temperature Gas-Phase Oxidation of n-Heptane and n-Decane. *J. Phys. Chem. A* **2017,** *121* (9), 1861-1876.
(29) Dagaut, P.; Reuillon, M.; Cathonnet, M., High-Pressure Oxidation of Liquid Fuels from Low to High-Temperature .1. N-Heptane and Isooctane. *Combust. Sci. Technol.* **1994,** *95* (1-6), 233-260.
(30) Zhang, Y.; Boehman, A. L., Oxidation of 1-butanol and a mixture of n-heptane/1-butanol in a motored engine. *Combust. Flame* **2010,** *157* (10), 1816-1824.
(31) Herbinet, O.; Husson, B.; Serinyel, Z.; Cord, M.; Warth, V.; Fournet, R.; Glaude, P. A.; Sirjean, B.; Battin-Leclerc, F.; Wang, Z. D.; Xie, M. F.; Cheng, Z. J.; Qi, F., Experimental and modeling investigation of the low-temperature oxidation of n-heptane. *Combust. Flame* **2012,** *159* (12), 3455-3471.
(32) Herbinet, O.; Husson, B.; Le Gall, H.; Battin-Leclerc, F., An experimental and modeling study of the oxidation of n-heptane, ethylbenzene, and n-butylbenzene in a jet-stirred reactor at pressures up to 10 bar. *Int. J. Chem. Kinet.* **2020,** *52* (12), 1006-1021.
(33) Al-Gharibeh, E.; Beyerlein, S.; Kumar, K., Speciation and Heat Release Studies during n-Heptane Oxidation in a Motored Engine. *Combust. Sci. Technol.* **2021**, 1-25.

TOC Graphic

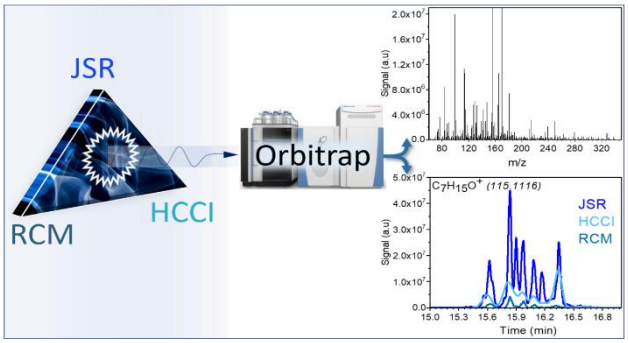
JSR
HCCI
RCM
Orbitrap
Signal (a.u)
m/z
$C_7H_{15}O^+$ (115.1116)
JSR
HCCI
RCM
Time (min)